

# Optical Characterizations and Preparations of Core-shell Type (Ag, Cu, and Ag-TiO<sub>2</sub>) and Hybrid Type (Ag-SiO<sub>2</sub>) Nanoparticles

(핵-껍질형 (Ag, Cu 및 Ag-TiO<sub>2</sub>)과 혼합형  
(Ag-SiO<sub>2</sub>) 나노입자의 합성과 광학적 특성)



A thesis submitted in partial fulfillment of the requirements  
for the degree of

Master of Science


in Department of Chemistry, The Graduate School,  
Pukyong National University

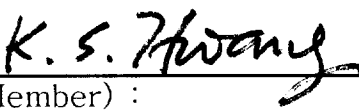
August, 2005

Optical Characterizations and Preparations of Core-shell Type (Ag, Cu, and  
Ag-TiO<sub>2</sub>) and Hybrid Type (Ag-SiO<sub>2</sub>) Nanoparticles

A Dissertation  
by  
Young Hwan Kim

Approved by :

  
\_\_\_\_\_  
(Chairman) :

  
\_\_\_\_\_  
(Member) :

  
\_\_\_\_\_  
(Member) :

August, 2005

# Contents

<b>1. Introduction .....</b>	<b>1</b>
<b>2. Experimentals .....</b>	<b>5</b>
<b>2-1. Materials and method .....</b>	<b>5</b>
2-1-1. Ag nanoparticles .....	5
2-1-1-1. Synthesis of Ag nanoparticles .....	5
2-1-1-2. Dispersibility and oxidation stability test of Ag nanoparticles .....	5
2-1-2. Ag-TiO <sub>2</sub> nanoparticles .....	6
2-1-2-1. Synthesis of Ag-TiO <sub>2</sub> nanoparticles I .....	6
2-1-2-2. Synthesis of Ag-TiO <sub>2</sub> nanoparticles II .....	7
2-1-3. Ag-SiO <sub>2</sub> nanoparticles .....	8
2-1-4. Synthesis of Cu nanoparticles .....	9
2-1-5. The test of antibiotic property .....	10
2-1-5-1. Antibiotic test by using Disk .....	11
2-1-5-2. Antibiotic test using UV-vis spectroscope .....	11
2-1-6. The test of deodorant property .....	13
<b>2-2. Background .....</b>	<b>13</b>
2-2-1. Sol-gel process .....	13
2-2-1-1. Solution chemistry of metal alkoxide precursors .....	13
2-2-1-2. Mechanisms of hydrolysis and condensation .....	14
2-2-1-3. Role of the catalyst .....	17
2-2-2. Antibiotic materials .....	18

2-2-3. Deodorant test using gas chromatography (GC) techniques .....	18
<b>2-3. Apparatus .....</b>	<b>19</b>
<b>3. Results and Discussion .....</b>	<b>20</b>
<b>3-1. Synthesized Ag nanoparticles .....</b>	<b>20</b>
3-1-1. TGA .....	20
3-1-2. XRD .....	20
3-1-3. UV-vis .....	21
3-1-4. EDS .....	22
3-1-5. TEM images .....	23
3-1-6. Test of dispersibility and oxidation stability .....	24
3-1-6-1. UV-vis data .....	24
3-1-6-2. TEM images .....	30
<b>3-2. Synthesized Ag-TiO<sub>2</sub> nanoparticles .....</b>	<b>33</b>
3-2-1. Synthesized Ag-TiO <sub>2</sub> nanoparticles I .....	33
3-2-1-1. TEM .....	33
3-2-1-2. UV-vis .....	33
3-2-1-3. EDS .....	35
3-2-2. Synthesized Ag-TiO <sub>2</sub> nanoparticles II .....	36
3-2-2-1. TEM .....	36
3-2-2-2. ED .....	36
3-2-2-3. UV-vis .....	37
3-2-2-4. XRD .....	38
3-2-2-5. EDX .....	39

<b>3-3. Synthesized Ag-SiO<sub>2</sub> nanoparticles</b>	40
3-3-1. TEM	40
3-3-2. High Resolution TEM images	42
3-3-3. UV-vis	43
3-2-4. EDS	43
3-3-4-1. TEM-EDS	43
3-3-4-2. SEM-EDS	45
<b>3-4. Synthesized Cu nanoparticles</b>	46
3-4-1. TGA	46
3-4-2. TEM	47
3-4-3. XRD	49
3-4-4. EDX	49
<b>3-5. Antibiotic test</b>	50
3-5-1. Ag nanoparticles	50
3-5-2. TiO <sub>2</sub> nanoparticles	51
3-5-3. Ag-TiO <sub>2</sub>	52
3-5-4. Ag-SiO <sub>2</sub>	52
3-5-5. Antibiotic property using UV-vis spectroscope	56
<b>3-6. Deodorant test</b>	58
3-6-1. Valeric acid	58
3-6-2. TiO <sub>2</sub>	58
3-6-3. Ag-TiO <sub>2</sub>	60
<b>4. Conclusion</b>	63

**5. References ..... 65**

**6. Korean abstract ..... 70**

## List of Figures

- Figure 2. 1      The synthetic process of Ag nanoparticles.
- Figure 2. 2      The process of dispersibility and oxidation stability test of Ag nanoparticles solution.
- Figure 2. 3      The synthetic process of Ag-TiO<sub>2</sub> nanoparticles I.
- Figure 2. 4      The synthetic process of Ag-TiO<sub>2</sub> nanoparticles II.
- Figure 2. 5      The synthetic route of Ag-SiO<sub>2</sub> nanoparticles.
- Figure 2. 6      The route of synthetic method of Cu nanoparticles.
- Figure 2. 7      The route of antibiotic test.
- Figure. 2. 8      Antibiotic test using disk ; (a) no existence of antibiotic property and (b) existence of antibiotic property.
- Figure 2. 9      The antibiotic test route utilizing UV-vis spectroscopy.
- Figure 2. 10     The peaks of antibiotic property using UV-vis spectroscopy. A : not being antibiotic property, B : being antibiotic property.
- Figure 2. 11     The experimental route of deodorant test.
- Figure 2. 12     AN (addition) mechanism similar to olation.

- Figure 2. 13      The mechanism of hydrolysis, alcoxolation and oxolation.
- Figure 2. 14      The mechanism of condensation.
- Figure 2. 15      The role of the acid catalyst.
- Figure 2. 16      The role of the base catalyst.
- Figure 3. 1        Weight loss for Ag-oleate complex during the heat treatment under air flow.
- Figure 3. 2        X-ray diffraction pattern (Cu K $\alpha$ -radiation) of Ag-oleate complex (A) and 300 °C aging of silver-oleate complex (B).
- Figure 3. 3        UV-vis spectrum of Ag nanocrystallites ( $\lambda_{\text{max}} = 411 \text{ nm}$ ).
- Figure 3. 4        Peaks for the element Ag is observed together with that for Si. The Si peak is due to the EDX detector.
- Figure 3. 5        TEM images of silver nanoparticles. The particle size is  $8.0 \pm 1.3 \text{ nm}$ .
- Figure 3. 6        UV-vis spectra of Ag nanoparticles in the passage of time.
- Figure 3. 7        UV-vis spectra of Ag nanoparticle sample 1 in the passage of time.



- Figure 3. 8      UV-vis spectra of Ag nanoparticle sample 3 in the passage of time.
- Figure 3. 9      UV-vis spectra of Ag nanoparticle sample 7 in the passage of time.
- Figure 3. 10     UV-vis spectra of Ag nanoparticle sample 8 in the passage of time.
- Figure 3. 11     The TEM image of first synthesized Ag nanoparticles.
- Figure 3. 12     The TEM images of first synthesized Ag nanoparticles after 70 days.
- Figure 3. 13     The TEM images of Ag nanoparticles after 23 days.
- Figure 3. 14     TEM images of Ag-TiO<sub>2</sub> nanoparticles in toluene (a), ethanol (b), water(c) and (d).
- Figure 3. 15     UV-vis spectra of Ag-TiO<sub>2</sub> nanoparticle.
- Figure 3. 16     EDS spectrum of Ag-TiO<sub>2</sub> nanoparticle.
- Figure 3. 17     TEM image of Ag-TiO<sub>2</sub> nanoparticles before (a) and after oleic acid coating and sonication (b).
- Figure 3. 18     ED pattern of Ag-TiO<sub>2</sub> nanoparticles before oleic acid coating and sonication (a) and after it (b).
- Figure 3. 19     UV-vis spectra of Ag nanoparticles ( $\lambda_{\text{max}} = 411 \text{ nm}$ , A)

and Ag- TiO<sub>2</sub> nanoparticles ( $\lambda_{\max} = 486$  nm, B).

- Figure 3. 20 X-ray diffraction pattern (Cu K $\alpha$ -radiation) of Ag-TiO<sub>2</sub> nanoparticles at annealing time and temperature (a) and confirmed with JCPSD cards (silver file no. 01-1164 and anatase titanium file no. 71-1169, underlined part) (b)
- Figure 3. 21 Energy-dispersive X-ray spectra of Ag-TiO<sub>2</sub> before oleic acid coating and sonication (a) and after it (b).
- Figure 3. 22 TEM image of Ag-SiO<sub>2</sub> nanoparticle : (a) SiO<sub>2</sub> nanoparticles size is determined as about 200 nm and (b) Ag nanoparticles size is below 10 nm.
- Figure 3. 23 Ag-SiO<sub>2</sub> nanoparticles prepared with different AgNO<sub>3</sub>. (a) : Ag : SiO<sub>2</sub> = 1 : 1, (b) : Ag : SiO<sub>2</sub> = 2 : 1, and (c) : Ag : SiO<sub>2</sub> = 3 : 1,
- Figure 3. 24 M-TEM image of SiO<sub>2</sub> nanoparticle deposited Ag nanoparticles.
- Figure 3. 25 Ag-SiO<sub>2</sub> nanoparticles prepared in water (a) and ethanol (b).
- Figure 3. 26 UV-vis spectra of Ag nanoparticle ( $\lambda_{\max} = 410$  nm) and Ag-SiO<sub>2</sub> nanoparticle ( $\lambda_{\max} = 420$  nm).
- Figure 3. 27 Energy-dispersive X-ray spectrum of Ag-SiO<sub>2</sub> nanoparticles.
- Figure 3. 28 TEM-EDS data of Ag-SiO<sub>2</sub> nanoparticles.

- Figure 3. 29      Measured and calculated value of Ag-SiO<sub>2</sub>.
- Figure 3. 30      SEM-EDS data of Ag-SiO<sub>2</sub> nanoparticles.
- Figure 3. 31      Measured and calculated value of Ag-SiO<sub>2</sub> of SEM-EDS.
- Figure 3. 32      TGA curve of different Cu-oleate complexes during heat treatment under air flow.
- Figure 3. 33      The formation of inner and outer layers of Cu-oleate complex.
- Figure 3. 34      Transmission electron micrographs of copper nanoparticles at different oleate concentrations (a) 0.05 M, (b) 0.1 M, (c) 0.2 M and (d) 0.3 M.
- Figure 3. 35      Transmission electron micrographs of copper nanoparticles at At the oleate concentration of 0.05 M. The particle size is determined as  $8.9 \pm 1.3$  nm.
- Figure 3. 36      X-ray diffraction pattern (CuK $\alpha$ -radiation) of copper-oleate complex at 300 °C.
- Figure 3. 37      Energy-dispersive X-ray spectra of copper nanocrystallites.
- Figure 3. 38      Antibiotic test of Ag nanoparticles. (a) Escherichia Coli (b) Staphylococcus Aureus.
- Figure 3. 39      Antibiotic test of TiO<sub>2</sub> nanoparticle. (a) Escherichia Coli (b) Staphylococcus Aureus.

- Figure 3. 40 Antibiotic test of Ag-TiO<sub>2</sub> nanoparticle. (a) Escherichia Coli and (b) Staphylococcus Aureus.
- Figure 3. 41 Clear zone figure of Ag-SiO<sub>2</sub>. (a) S. aureus, (b) P. aeruginosa, (c) C. albicans, (d) P. citrinum and (e) A. niger.
- Figure 3. 42 The result of antibiotic properties of AgSiO<sub>2</sub> nanoparticles. The concentration of AgSiO<sub>2</sub> nanoparticles ; (a): 0.02%; (b): 0.03%; (c):0.05% and (d):0.5%.
- Figure 3. 43 The result of antibiotic properties of AgSiO<sub>2</sub> nanoparticles. The concentration of Ag-SiO<sub>2</sub> nanoparticles ; (a): 0.05%; (b): 0.1%; and (c):0.2%.
- Figure 3. 44 Antibiotic test using Uv-vis. (B : bacterium, C : bacterium, D : Ag nanoparticle (0.2 g/200 ml) + bacterium, E : Ag nanoparticle (2 g/200 ml) + bacterium, F : TiO<sub>2</sub> nanoparticle (0.02 g/200 ml) + bacterium, G : TiO<sub>2</sub> nanoparticle (0.2 g/200 ml) + bacterium and F : Ag-TiO<sub>2</sub> nanoparticle (0.2 g/200 ml) + bacterium.)
- Figure 3. 45 Decrease of peak of valeric acid in the passage of time. (a) : 0 hrs and (b) : 24 hrs.
- Figure 3. 46 Decrease of peak of valeric acid contained TiO<sub>2</sub> nanoparticles in the passage of time. (a) : 0 hrs and (b) : 24 hrs.

Figure 3. 47      Decrease of peak of valeric acid contained Ag-TiO<sub>2</sub> nanoparticles in the passage of time. (a) : 0 hrs and (b) : 24 hrs.

## **List of Tables**

Table 2. 1	The comparison between organic and inorganic antibiotic agent.
Table 3. 1	Conditions of color changing test samples of Ag nanoparticles.
Table 3. 2	The ratio of Ag to Ti in Ag-TiO <sub>2</sub> nanoparticles.
Table 3. 3	Element and atomic ratio of Ag-TiO <sub>2</sub> nanoparticles before oleic acid coating and sonication treatment.
Table 3. 4	Ag to Si atomic% of Ag-SiO <sub>2</sub> nanoparticles of TEM-EDS.
Table 3. 5	Ag to Si atomic% of Ag-SiO <sub>2</sub> nanoparticles of SEM-EDS.
Table 3. 6	Clear Zone Value of Ag-SiO <sub>2</sub> .
Table 3. 7	Ag concentrations of Ag-SiO <sub>2</sub> nanoparticles.
Table 3. 8	The results of antibiotic properties of AgSiO <sub>2</sub> concentration.
Table 3. 9	MIC (%) of AgSiO <sub>2</sub> nanoparticles in various bacteria.
Table 3. 10	Value of area and percent of decrease of valeric acid in the passage of time.
Table 3. 11	Value of area and percent of decrease of valeric acid contained TiO <sub>2</sub> nanoparticles in the passage of time.

Table 3. 12      Value of area and percent of decrease of valeric acid  
                         contained Ag-TiO<sub>2</sub> nanoparticles in the passage of time.

Optical Characterizations and Preparations of Core-shell Type (Ag, Cu, and Ag-TiO<sub>2</sub>) and Hybrid Type (Ag-SiO<sub>2</sub>) Nanoparticles.

Young Hwan Kim

Department of Chemistry, Graduate School,  
Pukyong National University

**Abstract**

Ag and Cu nanoparticles of inorganic core-organic shell type were synthesized with thermal decomposition of Ag-oleate and Cu-oleate complex in autoclave. The synthesized Ag nanoparticles were used as seed of Ag-TiO<sub>2</sub> nanoparticles. Ag-TiO<sub>2</sub> nanoparticles were characterized with UV-vis spectrophotometer, transmission electron microscope, antibiotic property and so on. A room temperature route for doping silica particles with Ag nanoparticles to achieve hybrid structures was introduced. First, silica nanoparticles were synthesized according to the well-known Stöber method by hydrolysis and condensation of TEOS in a mixture of ethanol with water, using ammonia as catalyst to initiate the reaction. Second, Ag-SiO<sub>2</sub> nanoparticles were synthesized by reaction with AgNO<sub>3</sub> and SiO<sub>2</sub> nanoparticles. Also, the characterizations of Ag-SiO<sub>2</sub> nanoparticles were investigated with TEM images, X-ray powder diffractometer (XRD) spectrum, antibiotic property and so on.



## 1. Introduction

Nanoparticles is ultra fine particles which have the diameter from 1 nm to 100 nm and the properties of nanoparticles are different from those of macro materials. The synthesis of nanosized particle is a growing research field in chemical science, in accordance with the extensive development of nanotechnology.<sup>1-3</sup> The size-induced properties of nanoparticles enable the development of new applications or the addition of flexibility to existing systems in many areas, such as catalysis, optics, microelectronics and so on.<sup>4-7</sup> Mono and bimetallic particles in the nanosize regime find extensive applications in catalysis, since with reduced size, surface area increases leading to enhanced catalytic activity.<sup>8</sup> Various routes are available for the synthesis of capped metal nanoparticles.<sup>9</sup> These methods are based on the reduction process of precursor metal ions that include chemical reduction using different reducing agent, photoreduction, sonochemical and radiolytic methods.<sup>10-13</sup> Ag and Cu nanoparticles attracted considerable attention because of their catalytic, optical, and conducting properties.<sup>14-16</sup> Their syntheses have been achieved via various routes, including radiation methods, microemulsion techniques, supercritical techniques, sonochemical reduction, laser ablation, metal vapor synthesis, vacuum vapor deposition, chemical reduction, etc.<sup>17-19</sup> To avoid oxidation, these methods were usually performed in non-aqueous media, at low precursor concentration, and under an inert atmosphere. Using soluble polymers or surfactants as capping agents to prepare Ag and Cu nanoparticles in aqueous solutions is attractive because organic solvents are not used and the corresponding pollutants are absent. However, until now, only few works have been done because Ag and Cu is easily oxidized. Lisiecki et al and Joshi et al prepared Cu nanoparticles in aqueous solution of anionic surfactant sodium dodecyl sulfate, and various water-soluble polymers and surfactants under nitrogen atmosphere, respectively.<sup>14,20</sup> In this paper, Ag and Cu nanoparticles are synthesized by using thermal

decomposition method of Ag-oleate and Cu-oleate complex. This method has the advantages of dispersibility in organic solvent and reduction stability because of oleate coating on the surface. The merits of inorganic antibiotic materials is superior to that of organic antibiotic materials in durability, heat resistant, toxicity, selectivity and so on. The usefulness of silver and copper as an antimicrobial agent has been known for a long time. It is an effective agent with low toxicity, which is especially important in the topical antibacterial treatment.<sup>21</sup> Our final purpose is that Ag and Cu nanoparticles are applied to life environment as antibiotic materials. In the first place, we introduce new synthetic method of Ag and Cu nanoparticles prepared by using thermal decomposition of Ag-oleate and Cu-oleate complex. Novel optical effects are expected by appropriately arranging metal particles on the surface of insulating cores of spherical shape, so as to compose, on a nanometer scale, core-shell structures.<sup>22-24</sup> Optical resonance from near infrared to the visible range may be tuned by adjusting the core size, shell thickness and type of metal and core material.<sup>25-28</sup> Core-shell structures have been intensively studied very recently, in particular since such structures exhibit peculiar properties which make them attractive for applications in optical and biological sensors and in optoelectronics.<sup>29-32</sup> In all coating methods, the monolayer cover is important, as the chemistry is specific to the shell. The monolayer route to oxide-shell materials is rather involved and required multistep process, and scale-up is difficult. To this purpose, oxide nanospheres of nearly equal size, offering great flexibility of composition, are well suited.<sup>33-35</sup> While on planar substrates a number of vacuum-based deposition methods may be utilized, including physical and chemical vapor deposition, laser ablation and cluster beam deposition, and also thin coating techniques, the situation is different with non-planar substrates because of their peculiar geometry. This requires access of the deposit species not only from one, but from all directions which may be achieved in a gas stream or in solution. For practical reasons, solution methods, such as the deposition of nanoparticles from a colloidal route of

synthesis or particle formation directly on the surface by appropriate processes, are preferred. The first route includes electrostatic deposition of colloidal particles by means of adhesives such as polyelectrolytes covering the oxide surface and ligand-mediated immobilization of metal colloids on functionalized oxide surface.<sup>24,26</sup> The second route includes controlled chemical reduction, photochemical or radiation chemical, photocatalytic and sonochemical reduction.<sup>36-38</sup> The controlled reduction of precursor molecules on the oxide surface has two main advantages.<sup>39-41</sup> First, it avoids uncontrolled surface chemical interaction of the metal particles with functionalizing agents which may seriously influence the surface plasmon resonances.<sup>42-43</sup> Second, it allows control of the precursor size at moderate temperatures.<sup>44-45</sup> By varying the coating conditions such as pH, concentration, temperature and duration of exposure of the metal complex solution, the coverage of the oxide nanospheres and size of metal nanoparticles may be controlled.<sup>41</sup> As a synthetic route meeting the requirements of producing spectroscopically clear (no adhesives) and photochemically stable (no ligand) metal nanoparticle coating of silver on monodisperse Stöber silica nanospheres. Apart from temperature and the initial concentration of the metal precursor, there is not much scope for controlling nucleation and growth processes in the practical execution of this route. The aim of producing core-shell structures requires one to achieve a high nucleation but low growth rate, so as to obtain a high number density of metal nanoparticles without the formation of aggregates. Ag-SiO<sub>2</sub> nanoparticles was synthesized by using well-known Stöber method at low temperature route for coating SiO<sub>2</sub> nanoparticles with AgNO<sub>3</sub>. This synthesis was done completely without external reducing agents or media, adhesive aids or functionalizing agents. The usefulness of silver as an antimicrobial agent has been known for a long time. It is an effective agent with low toxicity, which is especially important in the topical antibacterial treatment.<sup>46-47</sup> During the past two decades, titania(TiO<sub>2</sub>) has received great attentions due to its unique photocatalytic activity in the treatment of

environmental contaminants. Numerous work have been carried out displaying its promising performance in degrading a wide variety of organic and inorganic pollutants.<sup>48-52</sup> In this study, the synthesized Ag nanopartiels were used as seed of Ag-TiO<sub>2</sub> nanoparticles which have Ag(core)-TiO<sub>2</sub>(shell) structures. This nanostructured materials composed of silver core of 10 - 20 nm diameter coated by titanium dioxide with less than 5 nm layer is produced by sol-gel process. The optical characterization of these nanoparticles were carried out with UV-vis spectrophotometer. The shape and morphology were investigated with transmission electron microscopy (TEM) and high resolution TEM. The lattice spacing were investigated with high resolution TEM and the ratio of components with energy dispersive X-ray (EDX). The decomposition of nanocomplex was analyzed with thermogravimetric analysis (TGA) and the crystallization process was studied with X-ray powder diffraction (XRD) instruments.

## 2. Experimentals

### 2-1. Materials and method

#### 2-1-1. Ag nanoparticles

##### 2-1-1-1. Synthesis of Ag nanoparticles

Silver nitrate ( $\text{AgNO}_3$ , 99+%) and sodium oleate (98%) were purchased from Aldrich Chemical Co. and used without further purification. The aqueous solutions contained sodium oleate (34.05 g, 0.1 mol) were stirred with 100 rpm at room temperature (R.T) for 2 hrs in distilled water (D.W, 1 L) and then silver nitrate (16.79 g, 0.1 mol) was added into oleate solution. This mixed solution was stirred with 100 rpm at room temperature for 6 hrs. After filtering and drying, Ag-oleate complex was transferred into the pyrex tube and immediately treated by heating to 300 °C at 2 °C/min for 2 hrs and more heating at 300 °C for 2 hrs, and then cooled at room temperature. Figure 2. 1 shows the synthetic process of Ag nanoparticles.

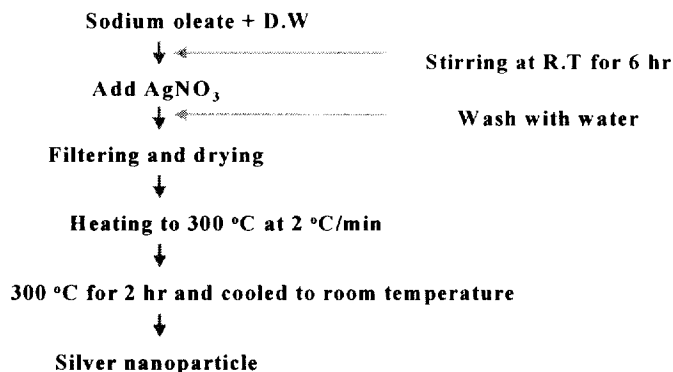


Figure 2. 1 The synthetic process of Ag nanoparticles.

#### 2-1-1-2. Dispersibility and oxidation stability test of Ag nanoparticles

The dispersibility and oxidation stability of Ag nanoparticles were examined with UV-vis spectroscopy and TEM. The morphology of TEM images and the peak shape of UV-vis of various concentration of Ag

nanoparticles solution were examined. Sample 1 was prepared by diluting Pure Ag nanoparticles solution (1 ml) with chloroform. Sample 2 was prepared by diluting sample 1 by adding chloroform. The concentration of sample 2 became half of concentration of sample 1. The same method was applied to make sample 3 and 4. Figure 2.2 shows the process of dispersibility and oxidation stability test of Ag nanoparticles solution.

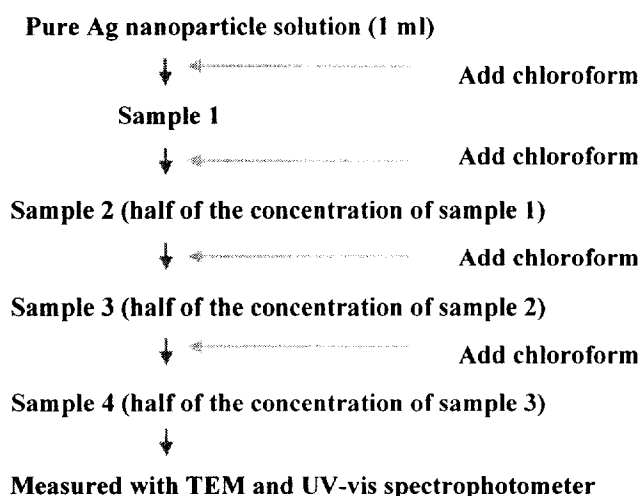


Figure 2.2 Dispersibility and oxidation stability test of Ag nanoparticles solution.

## 2-1-2. Ag-TiO<sub>2</sub> nanoparticles

### 2-1-2-1. The Synthesis of Ag-TiO<sub>2</sub> nanoparticles (method I)

Titanium(IV) butoxide (97%), acetylacetone (99+%), silver nitrate (99+%) and N,N-dimethylformamide (99.9+%) were purchased from Aldrich Chemical Co. and used without further purification. Ag-TiO<sub>2</sub> nanoparticles were synthesized by titanium colloids and silver colloids. A 100 ml titanium colloid was prepared by mixing of 0.34036 g titanium(IV) butoxide and 0.10012 g acetylacetone added with ethanol and treated with sonication for a few minutes. A 100 ml silver colloids was prepared by mixing of 0.16978 g silver nitrate and 0.1802 g H<sub>2</sub>O in N,N-dimethylformamide. As two

colloids were mixed and stirred at 90 °C for 2 hrs, colloids attained a green-black color. This mixture was cooled at room temperature. Figure 2. 3 shows the synthetic process of Ag-TiO<sub>2</sub> nanoparticles.

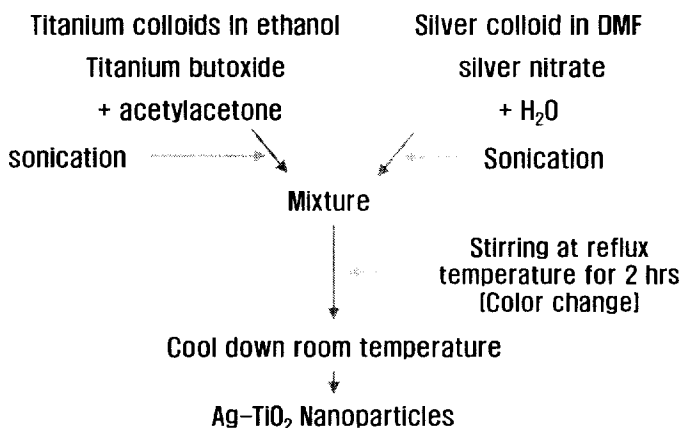


Figure 2.3 The synthetic process of Ag-TiO<sub>2</sub> nanoparticles I.

#### 2-1-2-2. The Synthesis of Ag-TiO<sub>2</sub> nanoparticles (method II)

Ag-TiO<sub>2</sub> nanoparticles were synthesized with titanium colloids and silver colloids. Titanium colloids are prepared by mixing of 0.34036 g titanium(IV) butoxide and 0.10012 g acetylacetone in ethanol and treated with sonication for a few minutes. A 100 ml silver colloids consisted of 1 ml Ag nanoparticles and chloroform were prepared by sonication of Ag nanoparticle solution. Ag nanoparticle prepared by thermal decomposition method was used. As two colloids were mixed and stirred at 90 °C for 2 hrs, mixed colloids changed to green-black. This product was cooled at room temperature. Figure 2. 4 shows the synthetic process of Ag-TiO<sub>2</sub> nanoparticles. To improve dispersibility, oleic acid (Aldrich Co., 99+%) was added into Ag-TiO<sub>2</sub> solution dissolved in ethanol.

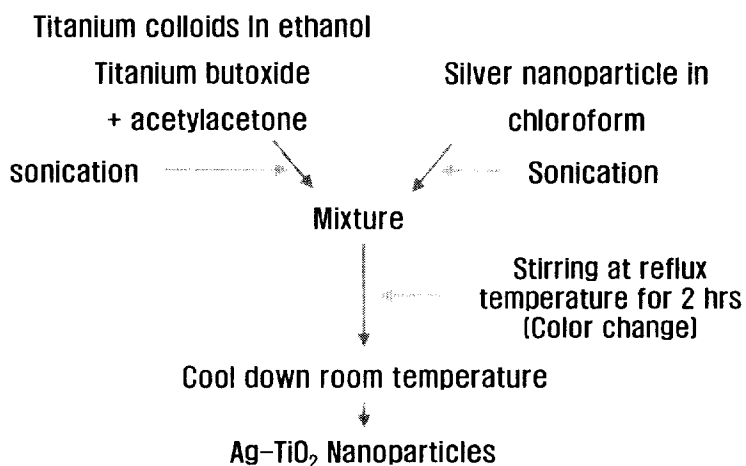


Figure 2. 4 The synthetic process of Ag-TiO<sub>2</sub> nanoparticles II.

### 2-1-3. Ag-SiO<sub>2</sub> nanoparticles

Silica nanoparticles were synthesized according to the well-known Stöber method by hydrolysis and condensation of tetraethoxysilane (TEOS, Aldrich Co., 98%) in a mixture of ethanol with water, using ammonia as catalyst to initiate the reaction. The size of silica nanoparticles is controlled by the molar ratio of TEOS, water and ammonia. The components were mixed with vigorous stirring for 6 hrs and finished by centrifugation. The separated products were dried at temperature below 100 °C for 2 hrs.<sup>53</sup> For the synthesis of Ag-SiO<sub>2</sub> nanoparticles, silver nitrate was added to silica solution. After the mixed solution was stirred for 6 hrs at room temperature, it was filtered, centrifuged and dried at room temperature for 2 hrs. Figure 2.5 shows the synthetic route of Ag-SiO<sub>2</sub> nanoparticles.



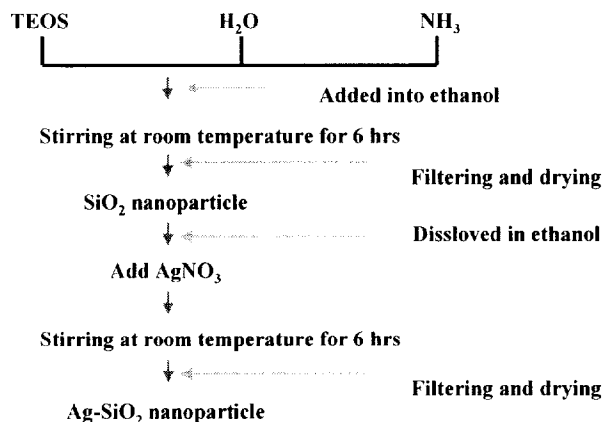


Figure 2. 5 The synthetic process of Ag-SiO<sub>2</sub> nanoparticles.

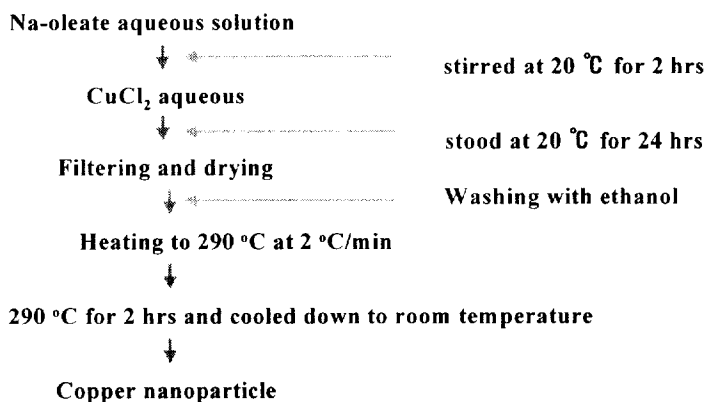


Figure 2.6 The synthetic process of Cu nanoparticles.

#### 2-1-4. Synthesis of Cu nanoparticles

Copper chloride (CuCl<sub>2</sub>, 99+%) and sodium oleate (98%) were purchased from Aldrich Chemical Co. and used without further purification. The 0.05 M, 0.1 M, 0.2 M and 0.3 M sodium oleate aqueous solutions were stirred at 20 °C for 2 hrs and then copper chloride solution was added into each oleate solution, respectively. After filtering and drying, Cu-oleate complex was transferred into the pyrex tubes and immediately treated by heating to 290 °C at 2 °C/min for 2 hrs and more heating at 290 °C for 2 hrs, and then cooled at room temperature. Figure 2.6 shows the route of synthetic

method of Cu nanoparticles.

#### 2-1-5. The test of antibiotic property

##### 2-1-5-1. Antibiotic test by using Disk

The antibiotic tests using UV-vis spectroscopy and disk plate were operated in shake chamber in the presence of ultraviolet and visible rays. In antibiotic test, two kinds of bacteria were used : *Escherichia Coli* (ATCC number 25922, negative) and *staphylococcus aureus* subsp (ATCC number 6538P, positive). The test route of antibiotic property using disk plate was shown in Figure 2. 7.. First, we select a bacteria and also select agar and broth according to selected bacteria. Broth and agar are giving nutrition to bacteria. Second, test disk plates and related apparatus are washed with ethanol and worked in asepsis room in existence of UV irradiation. Third, the selected bacteria were purified and cultivated. In this step, we confirmed that the selected bacteria consisted of one species and were not contaminated other bacteria. This process is important because infection of other bacteria in test bacteria was detected. The certificated test bacteria were dispersed in water solution contained Broth and reared in stirring chamber for 24 hrs. This solution was dropped into plate and placed in blacken chamber which was kept constant temperature for 48 hrs. Finally, we examined the antibiotic property. Figure 2. 7 is the route of antibiotic test. Figure 2.8 shows existence of antibiotic property. If there is no existence of antibiotic property, there is no signal.

##### 2-1-5-2. Antibiotic test using UV-vis spectroscopy

Figure 2. 9 is the antibiotic test route utilizing UV-vis spectroscopy. Like antibiotic test using disk, bacteria, agar and broth were selected. Samples contained 1 ml bacteria solution with antibiotic material (comparative sample) but the other without antibiotic material (reference sample) were

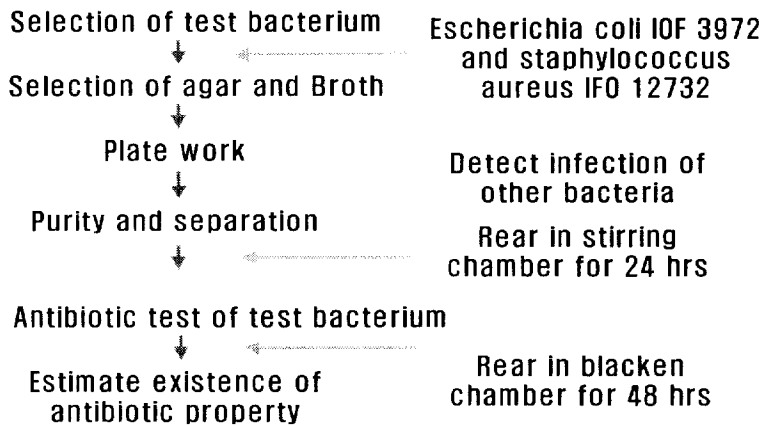


Figure 2.7 The route of antibiotic test.

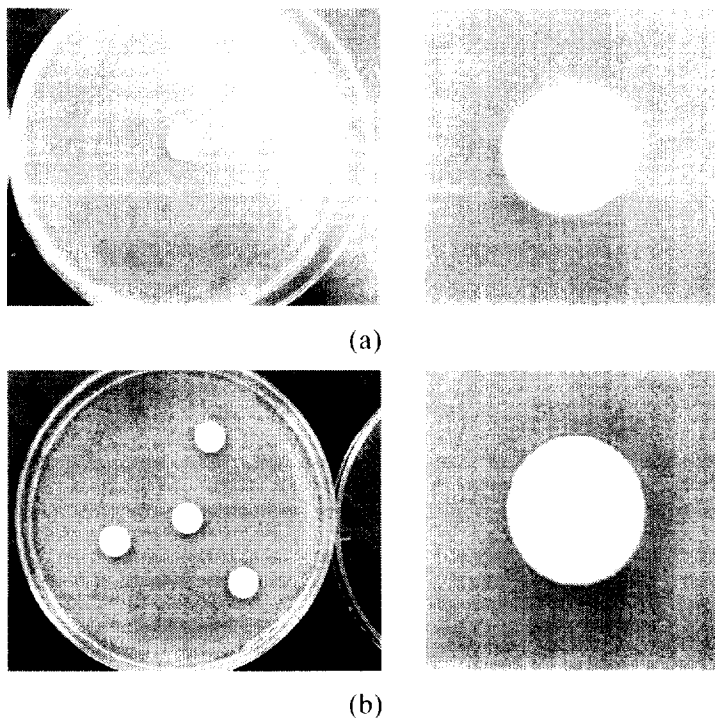


Figure. 2. 8 Antibiotic test using disk ; (a) no existence of antibiotic property and (b) existence of antibiotic property.

reared in shake chamber. Solution contained bacteria was examined at low

absorbance at 640 nm per 2 hrs by using UV-vis spectroscope. If bacteria have grown, the absorbance of solution become higher. Finally, absorbance of solution reached a plateau by saturation as shown in Figure 2. 10. Generally, bacteria grew like curve A in Figure 2. 10, but absorbance curves of materials with antibiotic properties show like Figure 2. 10 B.<sup>54-55</sup>

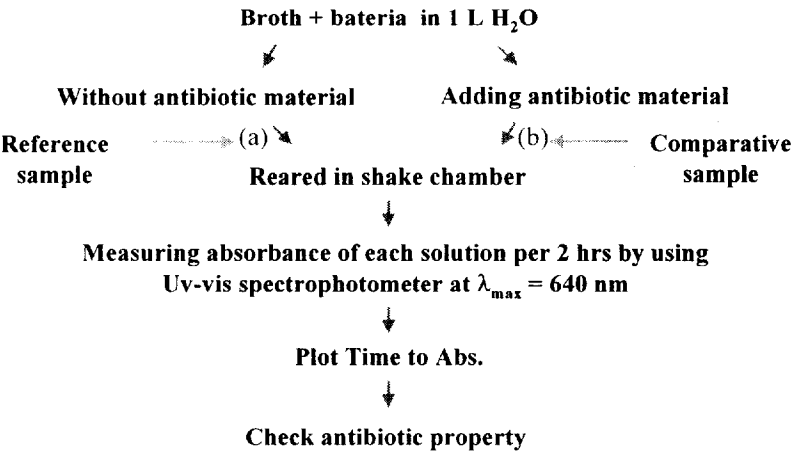


Figure 2.9 The antibiotic test route utilizing UV-vis spectroscope.

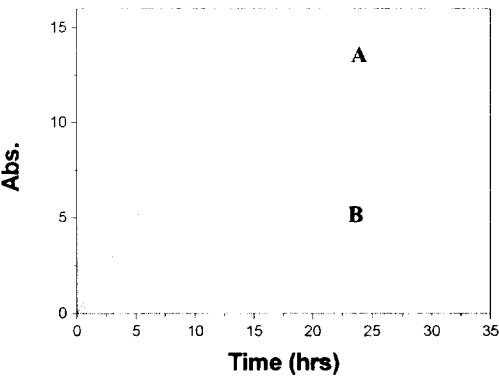


Figure 2. 10 The peaks of antibiotic property using UV-vis spectroscope.

A : not being antibiotic property, B : being antibiotic property

2-1-6. The test of deodorant property

Mainly, the deodorant test has been investigated with gas detector method but this method had disadvantages such as high expense, long time consuming and the leak of components. To overcome these disadvantages, we used the peaks of gas chromatography (GC). To investigate deodorant property, 10 ml valeric acid (99%, Aldrich Co.) which is the main factor of the stink of the feet was added into capsuled bottle. One sample contained only 10 ml valeric acid without deodorant material (comparative sample) but other samples with deodorant material (reference sample). The intensity and area of the peaks of each sample were measured every 2 hrs by GC. The experimental route of deodorant test is shown in Figure 2. 11.

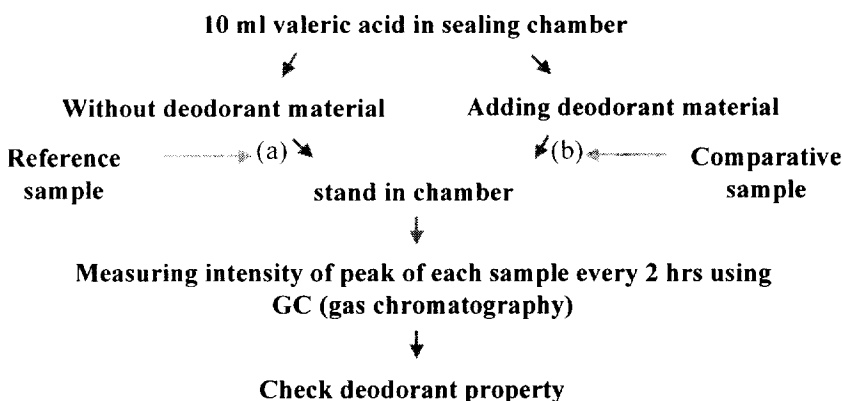


Figure 2.11 The experimental route of deodorant test

## 2-2. Background

### 2-2-1. Sol-gel process

#### 2-2-1-1. Solution chemistry of metal alkoxide precursors

Transition metal alkoxide,  $M(OR)_z$ , especially those of the  $d^0$  transition metals (Ti, Zr), are widely used as molecular precursors to glasses and ceramics. Metal alkoxides are in general very reactive due to the presence of highly electronegative OR groups (hard- $\pi$  donors) that stabilize M in its highest oxidation state and render M very susceptible to nucleophilic attack.<sup>56-57</sup> However, several factors distinguish transition metal alkoxides

from group IV silicon alkoxides ( $\text{Si(OR)}_4$ ), the most commonly used precursors in sol-gel processing.<sup>58</sup> (1) The lower electronegativity of transition metals causes them to be more electrophilic and thus less stable toward hydrolysis, condensation, and other nucleophilic reactions. (2) Transition metal often exhibit several stable coordinations, and when coordinatively unsaturated, they are able to expand their coordination via olation, oxolation, alkoxy bringing, or other nucleophilic association mechanisms. For example, transition metal alkoxides dissolved in nonpolar solvents often form oligomers via alkoxy bridging, an AN(addition) mechanism similar to olation;

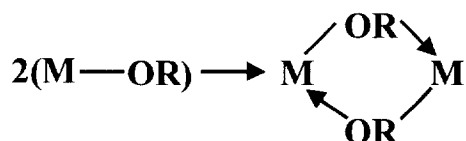


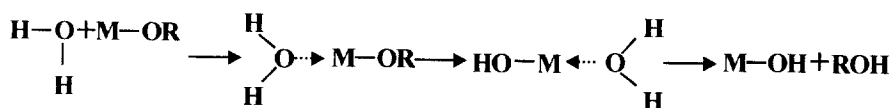
Figure 2. 12 AN (addition) mechanism similar to olation

In polar solvents such as alcohol, either alkoxy bridging or alcohol association can occur. (3) The greater reactivity of transition metal alkoxides requires that they be processed with stricter control of moisture and conditions of hydrolysis in order to prepare homogeneous gels rather than precipitates. (4) The generally rapid kinetics of nucleophilic reactions cause fundamental studies of hydrolysis and condensation of transition metal alkoxides to be much more difficult than for  $\text{Si(OR)}_4$ . In this regard it is noteworthy to study chemical and structural changes occurring at very short times.<sup>59</sup>

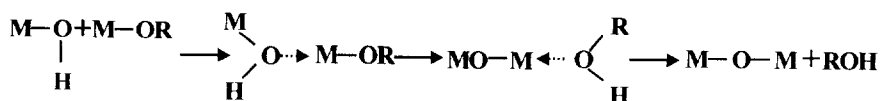
#### 2-2-1-2. Mechanisms of hydrolysis and condensation

For coordinatively saturated metals in the absence of catalyst, hydrolysis and condensation both occur by nucleophilic substitution ( $\text{S}_\text{N}$ ) mechanisms involving nucleophilic addition (AN) followed by proton transfer from the attacking molecule to an alkoxide or hydroxo-ligand in the transition state

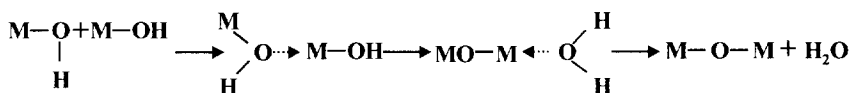
and removal of the protonated species as either alcohol (alcoxolation) and water (oxolation).<sup>60-61</sup> When coordination number (N) is larger than charge (z), condensation can occur by ololation. The thermodynamics of hydrolysis, alcoxolation and oxolation are governed by the strength of the entering nucleophile, the electrophilicity of the metal, and the partial charge and stability of the leaving group. These reactions are favored when  $\delta(O) \ll 0$ ,  $\delta(M) \gg 0$ , and  $\delta(H_2O)$  or  $\delta(ROH) > 0$ . Calculation of the charge distribution within the transition state of a titanate dimer pertaining to either oxolation or alcoxolation  $[Ti_2(OEt)_6(OH_2)]$  indicates that protonation of OEt produces a more positively charged leaving group ( $\delta(EtOH) = 0.02$ ) than protonation of OH ( $\delta(HOH) = -0.25$ ).<sup>56</sup> Thus alcoxolation should be the favored condensation reaction between partially hydrolyzed, coordinatively saturated titanate precursors. Since the transition state involves an associative mechanism accompanied by a proton transfer, kinetics are governed by the extent of coordination unsaturation of the metal N-z, and the transfer ability of the proton. Larger values of (N-z) and greater acidities of the protons reduce the associated activation barriers and enhance the kinetics. The thermodynamics of ololation depend on the strength of the entering nucleophile and the electrophilicity of the metal. The kinetics of ololation are systematically fast because  $(N-z) > 0$  and because no proton transfer occurs in the transition state. Another factor that influences reaction kinetics is the extent of oligomerization (molecular complexity) of the metal alkoxides. The



Hydrolysis



Alcoxolation



Oxolation

Figure 2. 13 The mechanism of hyrolysis, alcoxolation and oxolation.

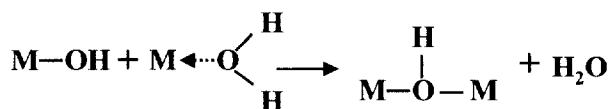
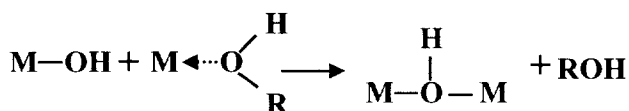


Figure 2. 14 The mechanism of condensation.

molecular complexity depends on the nature of the metal atom within a particular group, it increases with the atomic size of the metal alkoxides to polymerize rendering them insoluble.<sup>62</sup> Molecular complexity also depends on the alkoxide ligand. It is observed that alkoxy bridges are more stable toward hydrolysis than associated solvent molecules and in some cases terminal OR ligands. Therefore, starting from a particular alkoxide, the kinetics and resulting structure can be controlled by appropriate choice of solvent. The size and electron providing or withdrawing characteristics of the organic ligand also affect the hydrolysis and condensation kinetics, For a series of titanium n-alkoxides (Ti(OR<sup>n</sup>)<sub>4</sub>), the hydrolysis rate decreases with the alkyl chain length consistent with the steric effect expected for an associative S<sub>N</sub> reaction mechanism. Livage et al. show a trend of decreasing δ(Ti) and δ(H) with alkyl chain length that should also contribute to slower kinetics.

### 2-2-1-3. Role of the catalyst



Acid or base catalysts can influence both the hydrolysis and condensation rates and the structure of the condensed product. Acids serve to protonate negatively charged alkoxide groups, enhancing the reaction kinetics by producing good leaving groups, and eliminating the requirement for proton transfer within the transition state. Hydrolysis goes to completion when sufficient water is added. The relative ease of protonation of different alkoxide ligands can influence the condensation pathway. The ease of protonation decreases as alkoxy(M-OR), hydroxo(M-OH), oxo(M=O), which reflects the electron providing power of the ligands. Therefore acid catalyzed condensation is directed preferentially toward the ends rather than the middles of chains, resulting in more extended, less highly branched polymers.

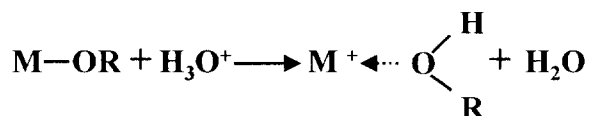


Figure 2. 15 The role of the acid catalyst.

Alkaline conditions produce strong nucleophiles via deprotonation of hydroxo ligands;

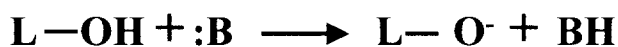


Figure 2. 16 The role of the base catalyst.

where L=M or H and B=OH<sup>-</sup> or NH<sub>3</sub>. Although base additions promote the hydrolysis of Si(OR)<sub>4</sub>, Bradley observed that the hydrolysis rate of Ti(OR)<sub>4</sub> was less in basic conditions (NaOH) than on acidic or neutral conditions, perhaps because nucleophilic addition of OH<sup>-</sup> reduces δ(Ti). Condensation kinetics are systematically enhanced under basic conditions. The order of reactivity toward nucleophilic attack should decrease as oxo, hydroxo, alkoxy. Thus base catalyzed condensation as well as hydrolysis should be directed toward the middles rather than the ends of chains, leading to more

compact, highly branched species.

### 2-2-2. Antibiotic materials

Organic antibiotic materials have been used for a long time. The merits of organic antibiotic materials are low cost and good miscibility but in spite of these merits, organic antibiotic materials have many disadvantages. Table show the comparison between organic and inorganic antibiotic agent.

**Table 2. 1 The comparison between organic and inorganic antibiotic agent.**

item	inorganic	organic	note
durability	semipermanent	2-4 months	Merits of inorganic antibiotic agent
Heat resistant	High (800 °C)	low	
toxicity	being	Not being	
MRSA inhibition	being	Not being	
selectivity	high	low	
reactivity	low	high	
stink	Not being	being	
Another effect	Far IR radiation effect	Not being	
cost	low	high	
miscibility	good	bad	

### 2-2-3. Deodorant test using gas chromatography (GC) techniques

Gas chromatography is a method for separating substances in a mixture and measuring the relative quantities of substances. It is a useful technique for substances that do not decompose at high temperatures and when a very small quantity of sample (micrograms) is available. In this type of chromatography, a sample is rapidly heated and vaporized, and then a stream of gas carries it along a column that contains a stationary phase. The sample becomes distributed between the mobile gas phase and the stationary phase. The higher a substance's affinity for the stationary phase, the more slowly it comes off of the column. From retention time which is eigenvalue to components, we can analyze qualitative analysis of materials

form retention time and quantitative analysis of materials from height and area of peak. From GC method, we can analyze deodorant materials exactly.

### **2-3. Apparatus**

Structural characterization of the products was done with transmission electron microscopes (TEM, HITACHI H-7500 and high resolution TEM, JEOL JEM 2010). X-ray powder diffraction (XRD, Philips X'pert-MPD system) and UV-vis spectrophotometer (HITACHI U-2001). The prepared nanoparticles were characterized by transmission electron microscopes energy dispersive X-ray (TEM-EDX, JEOL JEM 2010), scanning electron microscope energy dispersive X-ray (SEM-EDS, Hitachi S-2400) and electron probe X-ray micro analyzer (EPDM, shimazu EPDM-1600). The decomposition of Cu-oleate complex was analyzed with thermogravimetric analysis (TGA, Perkin-elmer TGA 7). The antibiotic test using UV-vis spectroscope was operated in shake chamber in the presence of ultraviolet and visible rays. Deodorant test was operated with gas chromatography (GC, GC(FID)/MS QP-5050A with Tekmar Autocan System).

### 3. Results and Discussion

#### 3-1. Synthesized Ag nanoparticles

##### 3-1-1. TGA

The decomposition path of the silver-oleate complex was studied by TGA analysis. Figure 3. 1 shows weight loss for silver-oleate complex during heat treatment under air flow. A very strong endothermic peak was observed at 295 °C. The peak was related to the evaporation of oleate molecules by the decomposition of silver-oleate complex. The weight loss occurred at 220 °C due to decomposition of CTAB.<sup>63</sup>

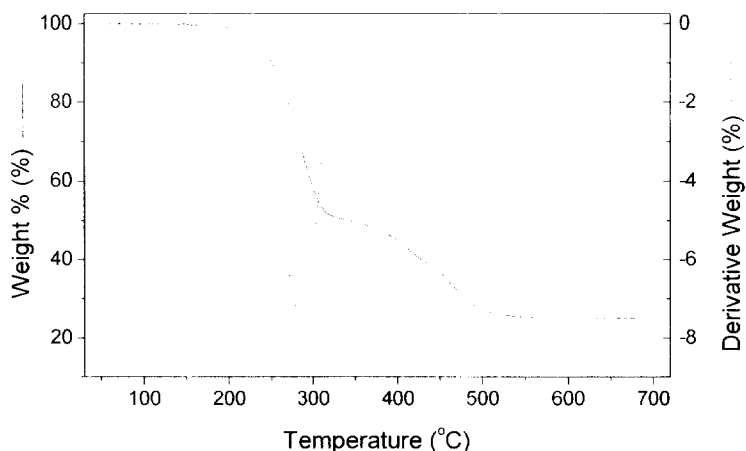


Figure 3.1 Weight loss for Ag-oleate complex during heat treatment under air flow.

##### 3-1-2. XRD

Figure 3. 2 illustrates the XRD pattern of silver-oleate complex curve (A) and silver-oleate complex aged at 300 °C curve (B). No peak of silver in the pristine silver-oleate complex was observed in the XRD analysis. This indicated that the complex was amorphous. However, peaks of silver was

observed in the silver-oleate complex aged at 300 °C. Peaks are broad due to the nanocrystalline size of silver. Curve B shows three peaks at 2 theta values of 38.2°, 44.5° and 64.5° corresponding to (111), (200) and (220) planes of silver, respectively. No impurity peak was observed in the XRD spectrum.

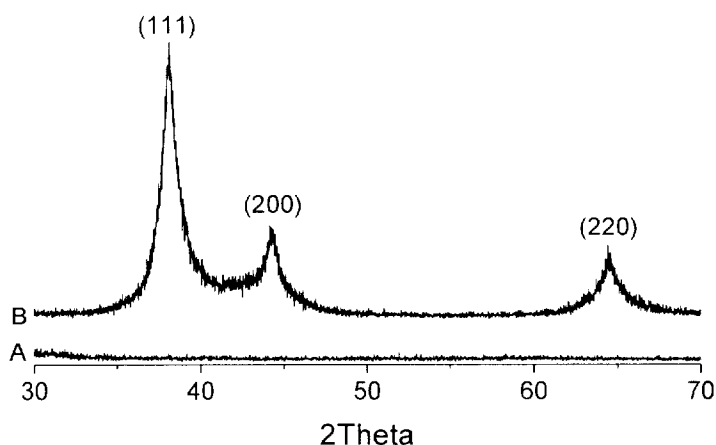


Figure 3.2 X-ray diffraction pattern (Cu K $\alpha$ -radiation) of Ag-oleate complex curve A and the silver-oleate complex aged at 300 °C (B). The diffraction peaks are indexed to (111), (200), and (220) planes at silver crystal structure. The crystal size determined by Debye-Scherrer equation with XRD data was 10.6 nm.

### 3-1-3. UV-vis spectroscopy

Figure 3. 3 shows UV-vis spectrum of Ag nanoparticle ( $\lambda_{\text{max}} = 411 \text{ nm}$ ) dispersed in chloroform solution. The optical absorption band at about 400 nm ( $\sim 3\text{eV}$ ) is typical of absorption at metallic Ag nanoparticle due to the surface plasmon resonance (SPR).<sup>64</sup> The colloidal suspensions of silver particles were a bright yellow-greenish color due to the intense bands around the excitation of SPR.<sup>65</sup> Although the conduction and valence bands of semiconductors are separated by a well-defined band gap, metal

nanoparticles have close-lying bands and electrons move quite freely. The free electrons give rise to a surface plasmon absorption band on the surface of metal particles, which depends on both the particle size and chemical surroundings. This absorption band is a little red-shifted and symmetric shape compared with the plasmon absorption band of silver colloids prepared by citrate reduction method.<sup>66</sup> It is caused that silver nanoparticles have narrower size-distribution and a little bigger diameter than silver nanoparticles prepared by citrate reduction method.

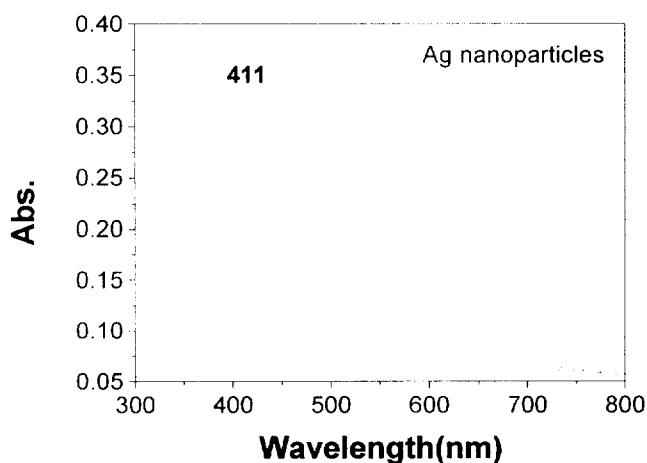


Figure 3. 3 UV-vis spectrum of Ag nanocrystallites ( $\lambda_{\max}=411$  nm).

#### 3-1-4. EDS

Figure 3. 4 shows the EDS spectra of silver nanoparticles excited by an electron beam (200 kV). Peaks for the elements of Ag and Cu were observed together. The Cu peaks are due to the 400 mesh copper grid. There is no impurity in the nanoparticles except silver atom. Accordingly, from the EDS spectra we could confirm that the nanoparticles in TEM images are pure silver particles.

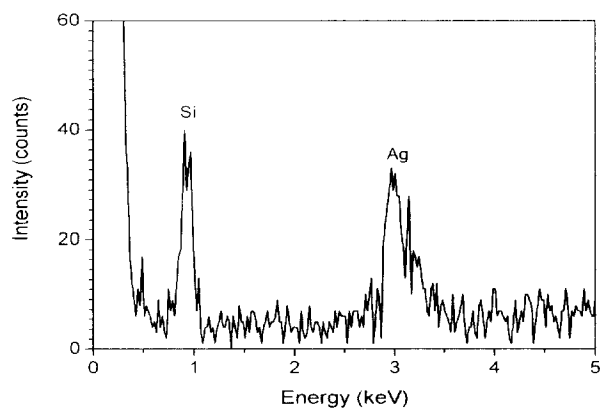


Figure 3. 4 Peaks for the element Ag is observed together with that for Si. The Si peak is due to the EDX detector.

### 3-1-5. TEM images

Figure 3. 5 is TEM images of monodisperse nanoparticles of silver. Most of the silver particles are spherical. The mean size of silver nanoclusters was determined as  $8.0 \pm 1.3$  nm. This means that the silver nanoparticles have very narrow size distribution

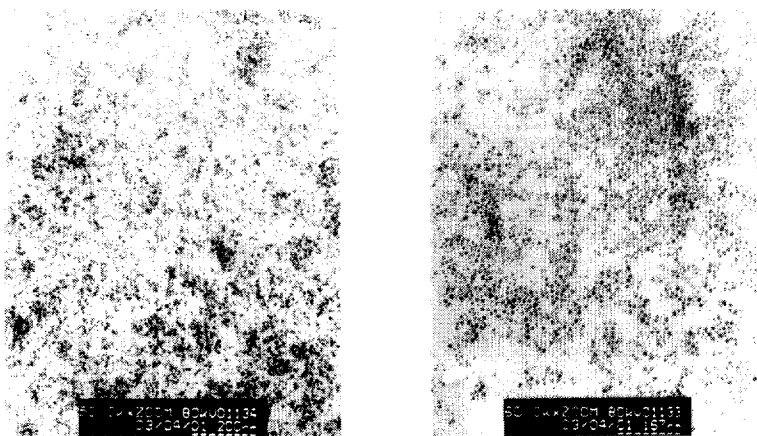


Figure 3. 5 TEM images of silver nanoparticles. The particle size is  $8.0 \pm 1.3$  nm.

### 3-1-6. Test of dispersibility and oxidation stability

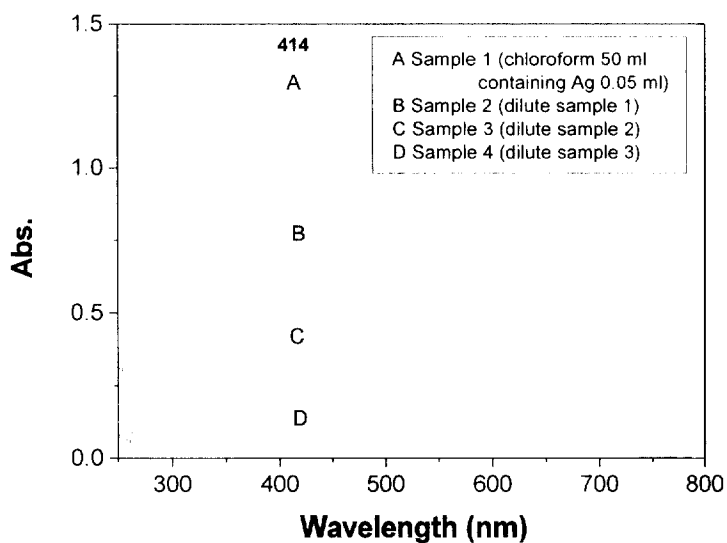
#### 3-1-6-1. UV-vis data

In case of allowance of light and air, the shoulder peak of UV-vis disappeared with decreasing the concentration of Ag colloids but the intensity of UV-vis peak decreased and finally disappeared. This is due to that Ag nanoparticles are aggregated and the size of Ag nanoparticles increased at the cost of decreasing the number of Ag nanoparticles (concentration of Ag colloid). In case of sample 1, shoulder peak appeared after 3 days, the width of UV-vis peak increased and the intensity of UV-vis decreased in accordance with passage of time. Sample 2 also shows the same pattern of sample 1, but shoulder peak appeared after 5 days, but sample 3 and 4 do not show shoulder peak. After excluding only light, the shoulder peak of sample 6 appeared after 11 days and the decrease of intensity of UV-vis peak is shown. After excluding only air, the shoulder peak of sample 7 is not shown clearly after 30 days but the half width of peak increased and the decrease of intensity of UV-vis peak is shown. After excluding light and air, there is no shoulder peak in sample 8 after 30 days, but the half width of peak somewhat increased. There is also decrease of intensity of UV-vis peak. As the passage of time, in the high concentration of Ag nanoparticle colloids, the shoulder peak is detected early compared to low concentration of Ag nanoparticles colloid. In the case of excluding air (sample 7 and 8), there is no shoulder peak. Supply of chloroform has an affect on this phenomenon because, in case of permitting air like sample 1-5 and 6, chloroform which is very volatilizable was added to the Ag nanoparticle colloids. If Ag nanoparticles is capped with oleate, there is no aggregation, but if chloroform is added to Ag nanopartilce colloids, the oleate capping Ag nanoparticles is removed and finally, the aggregation of Ag nanoparticles is occurred.

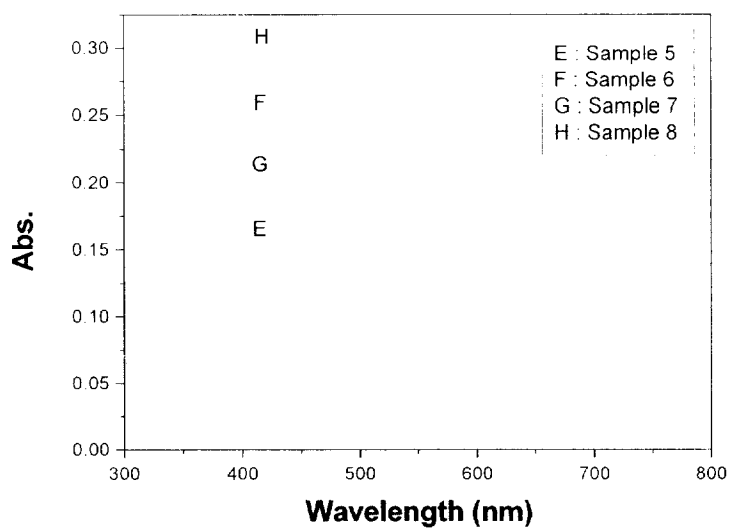


**Table 3. 1 Conditions of color changing test samples of Ag nanoparticles.**

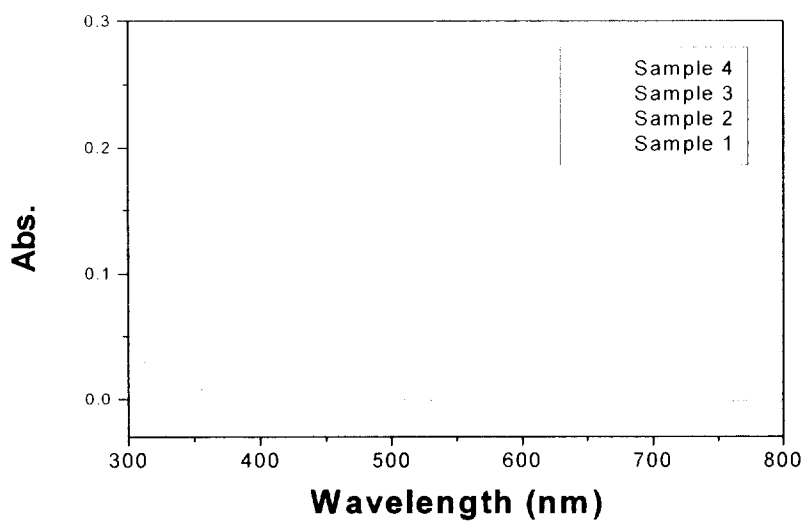
No.	Abs.	Note								
		Air	Light	2 days	4 days	7 days	11 days	14 days	23 days	30 days
1	414	allow	allow	413	414	414	413	413	419	409
2	414	allow	allow	412	414	412	416	421	411	412
3	414	allow	allow	415	415	414	420	415	411	-
4	414	allow	allow	412	415	415	414	409	-	-
5	414	allow	allow	416	414	414	416	412	411	-
6	414	allow	forbidden	416	414	416	420	420	411	417
7	414	forbidden	allow	415	414	414	414	415	411	417
8	414	forbidden	forbidden	416	415	415	415	415	411	417



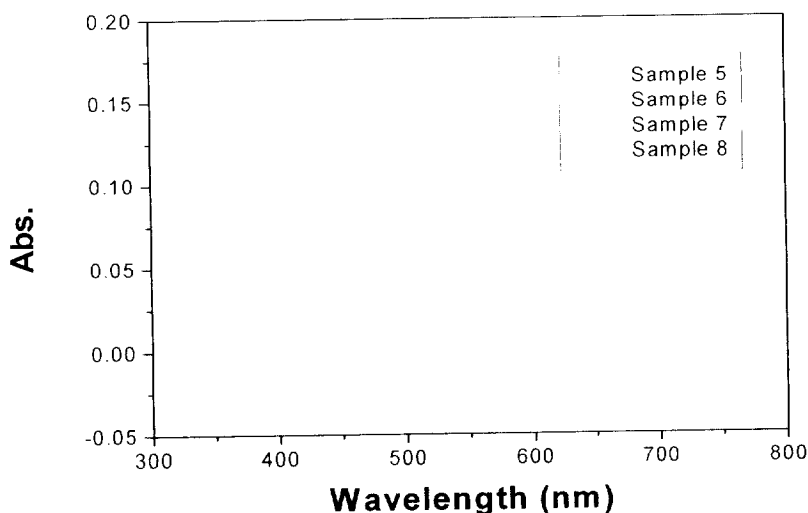
(a) The UV-vis spectra of samples 1-4 after 1 days



(b) The UV-vis spectra of samples 5-8 after 1 days



(c) The UV-vis spectra of samples 1-4 after 30 days



(d) The UV-vis spectra of samples 5-8 after 30 days

Figure 3. 6 UV-vis spectra of Ag nanoparticles in the passage of time.

Figure 3. 7 shows the intensity of UV-vis decreased and the shoulder peak increased. The intensity of  $\lambda_{\max}$  in the UV-vis spectra of sample 3 in Figure 3. 8 decreased and the shoulder peak appeared after 23 days and absorbance was not detected after 30 days. The intensity of  $\lambda_{\max}$  in UV-vis spectra of sample 7 in Figure 3. 9 decreased, but there was no shoulder peak and the half width of  $\lambda_{\max}$  of UV-vis spectra increased. The intensity of UV-vis spectra of sample 8 in Figure 3. 10 decreased but there was no shoulder peak and the half width of  $\lambda_{\max}$  of UV-vis spectra increased. If there were larger size distributions in colloid, the half width of UV-vis spectra increased and the shapes of spectra were broad. If colloid consisted of small size distributions, the half width of UV-vis spectra was narrow and the shapes of spectra were very sharp.

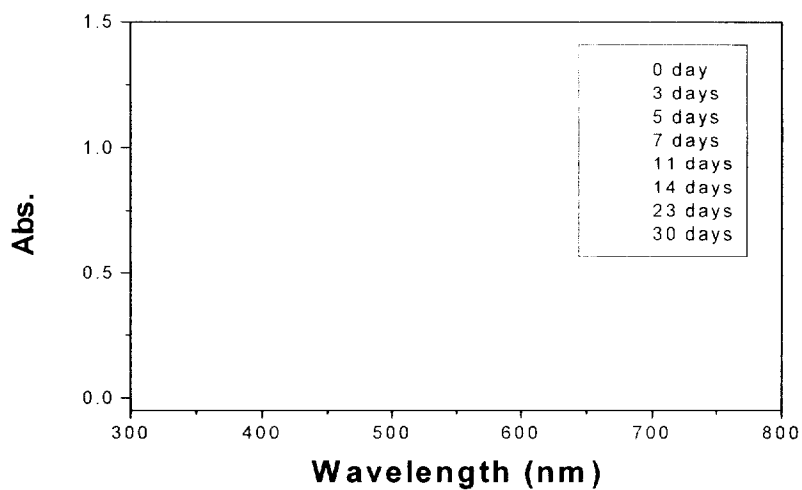


Figure 3. 7 UV-vis spectra of Ag nanoparticle sample 1 in the passage of time.

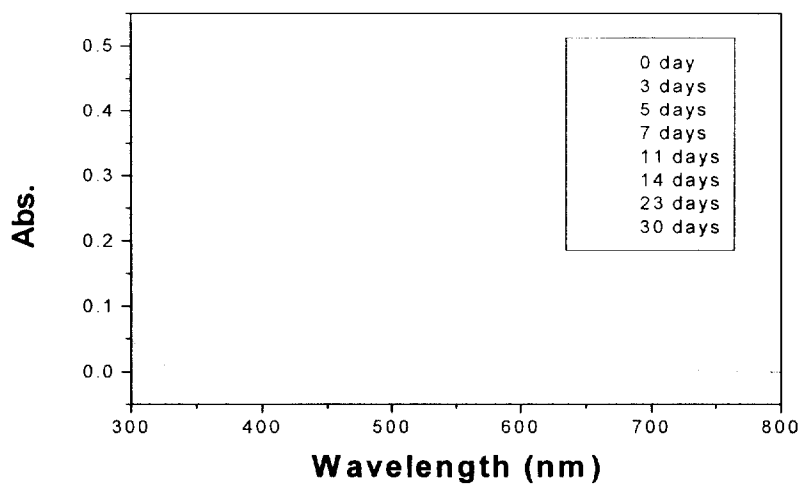


Figure 3. 8 UV-vis spectra of Ag nanoparticle sample 3 in the passage of time.

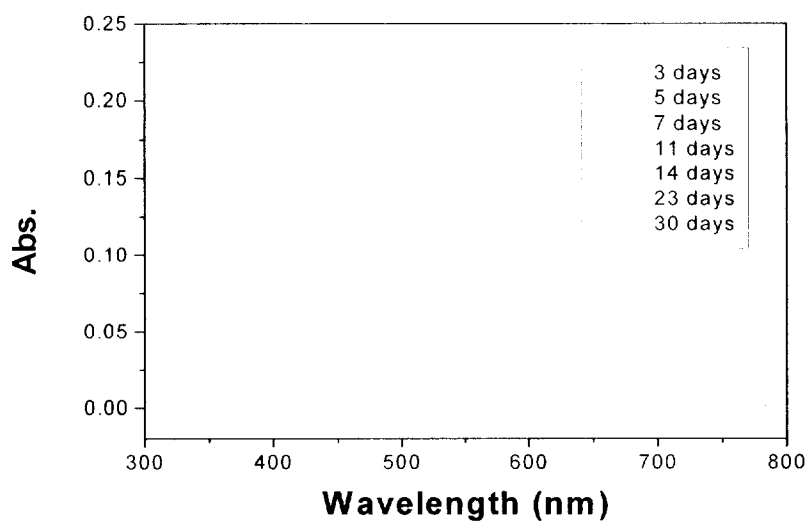


Figure 3. 9 UV-vis spectra of Ag nanoparticle sample 7 in the passage of time.

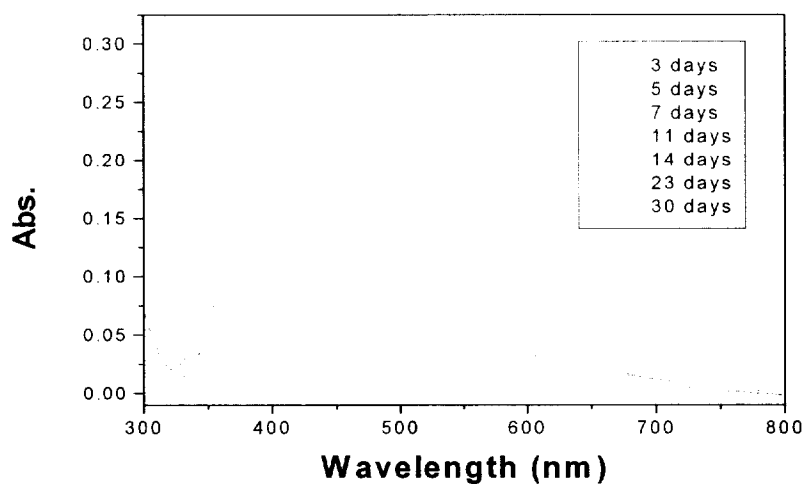


Figure 3. 10 UV-vis spectra of Ag nanoparticle sample 8 in the passage of time.

### 3-1-6-2. TEM images

After 70 days, the synthesized Ag nanoparticles have good dispersibility in chloroform, but samples 1-8 have more aggregation of Ag nanoparticles and larger size distribution as passage of time. Samples 1-6 has large size distribution but the size distributions of sample 7 and 8 are smaller than that of sample 1-6 because in cases of samples 1-6, chloroform which is very volatilizable added to Ag nanoparticle colloids. If Ag nanoparticles is capped with oleate, there is no aggregation, but if chloroform is added to Ag nanoparticle colloids, the oleate capping Ag nanoparticles is removed and finally, the aggregation of Ag nanoparticles is occurred.

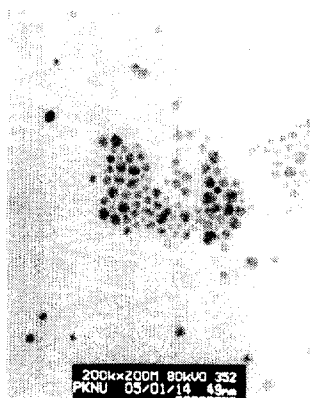
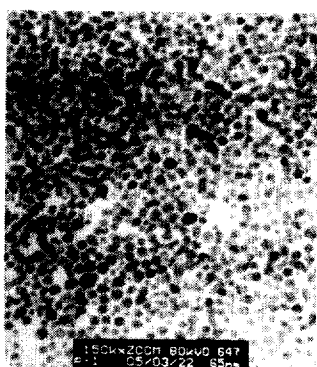
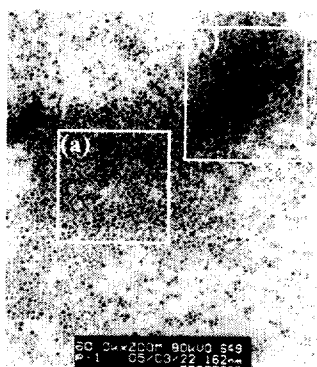
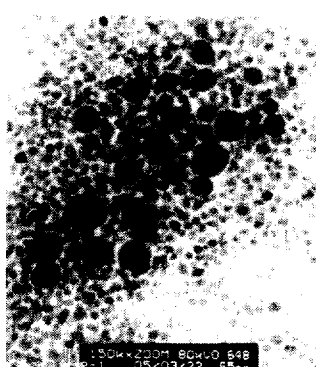


Figure 3. 11 The TEM image of first synthesized Ag nanoparticles.

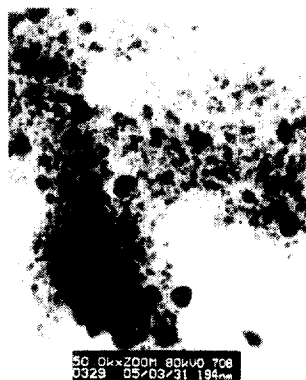


(a)

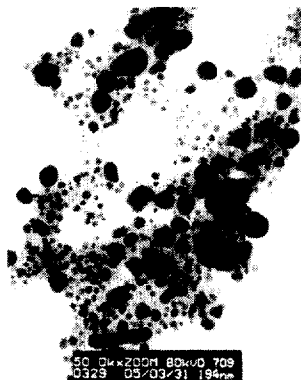


(b)

Figure 3. 12 The TEM images of first synthesized Ag nanoparticles after 70 days.



(a) sample 1



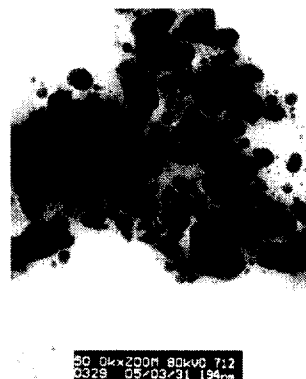
(b) sample 2



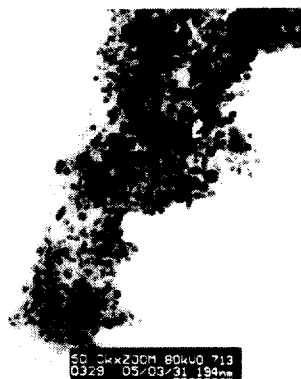
(c) sample 3



(d) sample 4



(e) sample 5



(f) sample 6



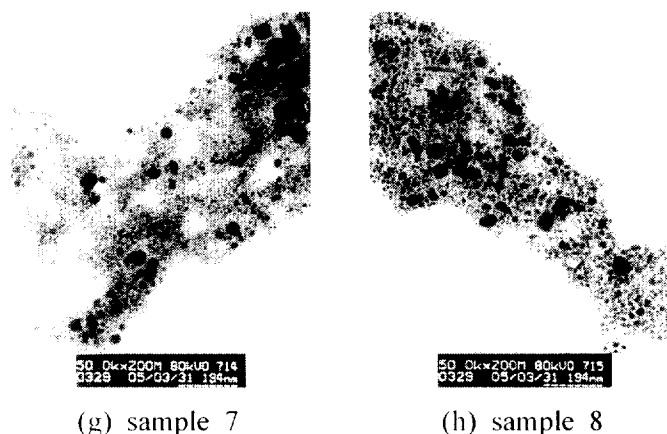


Figure 3. 13 The TEM images of Ag nanoparticles after 23 days.

## 3-2. Synthesized Ag-TiO<sub>2</sub> nanoparticles

### 3-2-1. Synthesized Ag-TiO<sub>2</sub> nanoparticles (method I)

#### 3-2-1-1. TEM

Figure 3. 14 shows TEM images of aggregated Ag nanoparticles coated with TiO<sub>2</sub> in ethanol but these images do not show core-shell formation clearly and also maintain these formation after adding dispersive agent and sonication treatment.

#### 3-2-1-2. UV-vis spectroscopy

UV-vis spectra of Ag-TiO<sub>2</sub> nanoparticle was also shown in Figure 3. 15. UV-vis spectrum of Ag-TiO<sub>2</sub> nanoparticle shows absorption band at 420 nm in ethanol and 452 nm in water but no absorption band in toluene where as UV-vis spectrum of Ag nanoparticles prepared using thermal decomposition method shows at 411 nm. This absorption band is rather broad and red-shifted compared with the plasmon absorption band of Ag nanoparticle.

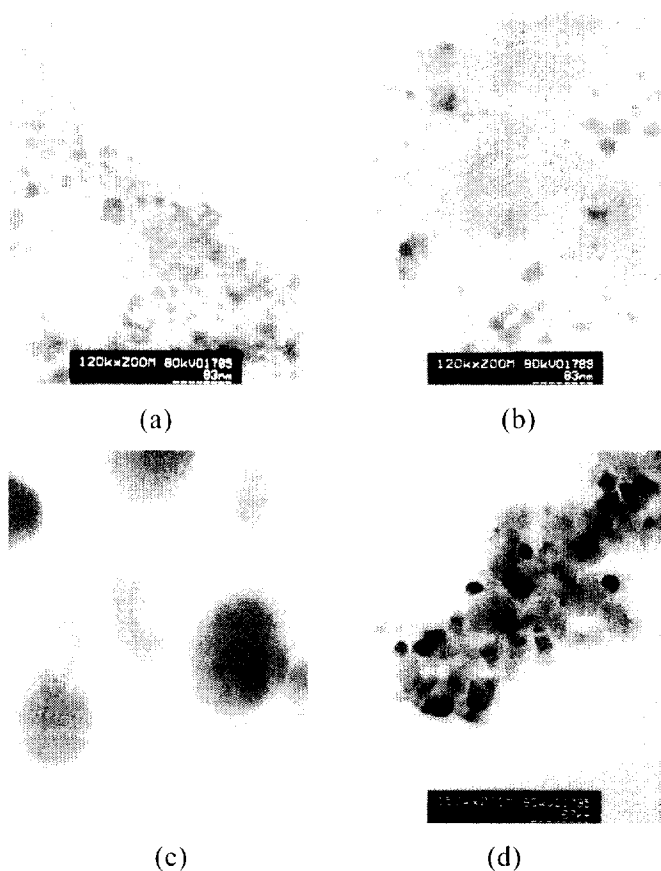


Figure 3. 14 TEM images of Ag-TiO<sub>2</sub> nanoparticles in toluene (a), ethanol (b), water(c) and (d).

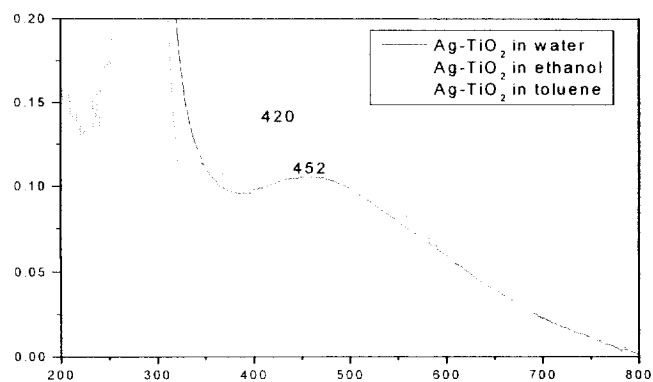


Figure 3. 15 UV-vis spectra of Ag-TiO<sub>2</sub> nanoparticle.

### 3-2-1-3. EDS

EDX data in Figure 3. 16 show that this nanoparticles consist of Ag and Ti components. The atomic ratio of Ag to Ti is 83.07 to 16.93 in Table 3. 2.

**Table 3.2 The ratio of Ag to Ti in Ag-TiO<sub>2</sub> nanoparticles.**

	Element (%)	Atomic (%)
Ti	68.54	83.07
Ag	31.46	16.93
Total	100.00	100.00

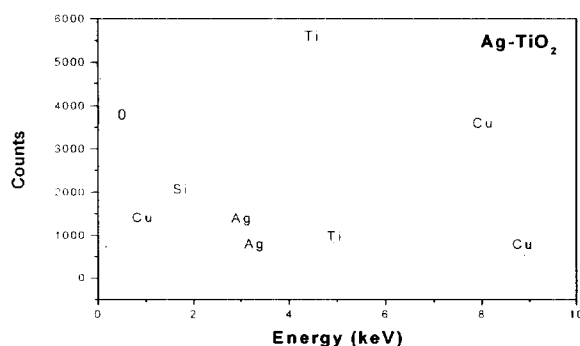


Figure 3. 16 EDS spectrum of Ag-TiO<sub>2</sub> nanoparticle.

### 3-2-2. Synthesized Ag-TiO<sub>2</sub> nanoparticles (method II)

#### 3-2-2-1. TEM

Figure 3. 17 shows TEM images of aggregated Ag nanoparticles coated with TiO<sub>2</sub>. This product was redispersed in ethanol solvent containing oleic acid and treated with sonication. Figure shows well dispersed Ag-TiO<sub>2</sub> nanoparticles treated with sol-gel process. The oleic acid as amphiphile has a C<sub>18</sub> tail with a cis-double bond in the middle, forming a kink. Such kinks have been postulated as necessary for effective stabilization. The oleic tails were solvated and fully wetted by the liquid medium, This is probably due to the kink in the oleic surfactant tail, which weakens their nematic

attraction and thus favors their solvation.<sup>67-68</sup> High resolution TEM image shows that the nanoparticles have about 13 nm Ag core and 2 nm TiO<sub>2</sub> shell structures.

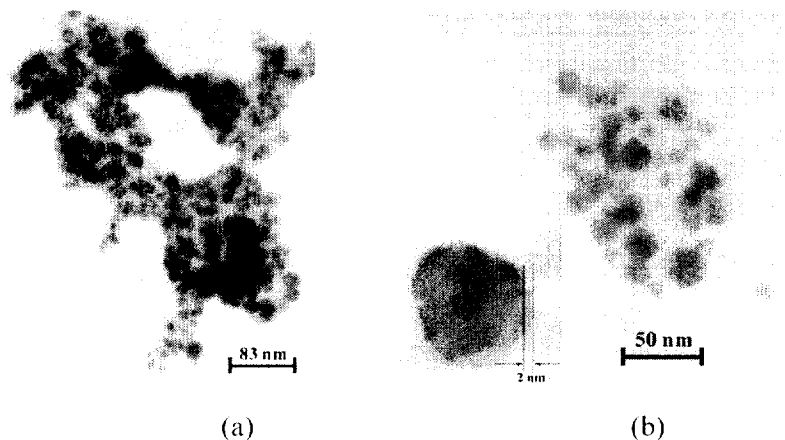


Figure 3. 17 TEM image of Ag-TiO<sub>2</sub> nanoparticles before (a) and after oleic acid coating and sonication (b).

### 3-2-2-2. Electron Diffraction (ED)

ED pattern of Ag- TiO<sub>2</sub> nanoparticles as shown in Figure 3. 18 is identical with that of Ag nanoparticles. The ED pattern of Ag nanoparticles is not shown in Figure 3. 18 (a) due to amorphous TiO<sub>2</sub> layer. After Ag-TiO<sub>2</sub> nanoparticles are coated with oleic acid and treated with sonication, ED pattern of Ag-TiO<sub>2</sub> nanoparticles becomes clear. This means that TiO<sub>2</sub> attached on surface of Ag nanoparticles is partly eliminated.

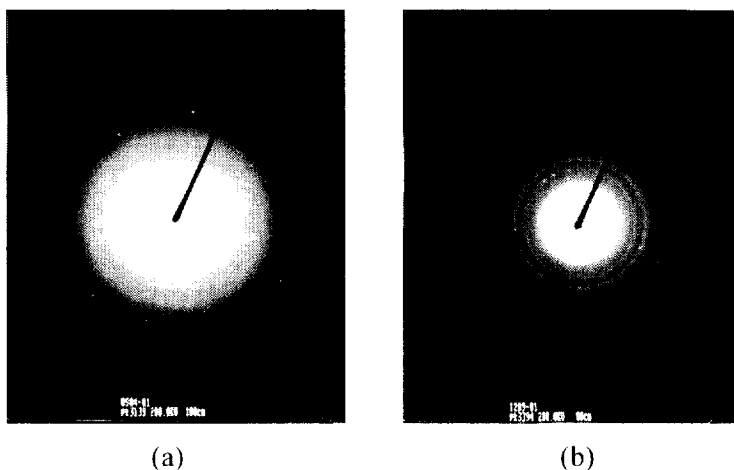


Figure 3. 18 ED pattern of Ag-TiO<sub>2</sub> nanoparticles before (a) and after (b) coating of oleic acid and sonication.

### 3-2-2-3. UV-vis spectroscopy

UV-vis spectra of Ag-TiO<sub>2</sub> nanoparticle are also shown in Figure 3. 19. UV-vis spectrum of Ag-TiO<sub>2</sub> nanoparticle shows  $\lambda_{\text{max}}$  at 486 nm where as UV-vis spectrum of Ag nanoparticles prepared shows  $\lambda_{\text{max}}$  at 411 nm. This absorption band is more broad and red-shifted compared with the plasmon absorption band of Ag nanoparticle. As discussed earlier, the position and shape of the plasmon absorption of silver nanoparticles are strongly dependent on the particle size, dielectric medium, and surface-adsorbed species.<sup>69-70</sup> Before and after oleic acid coating and sonication treatment, absorption band of UV-vis spectrum is not shifted. It indicates that absorption band of UV-vis spectrum is independent of oleic acid coating.

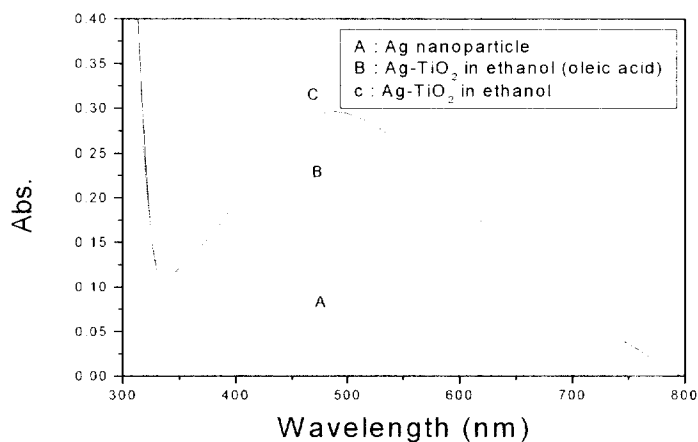
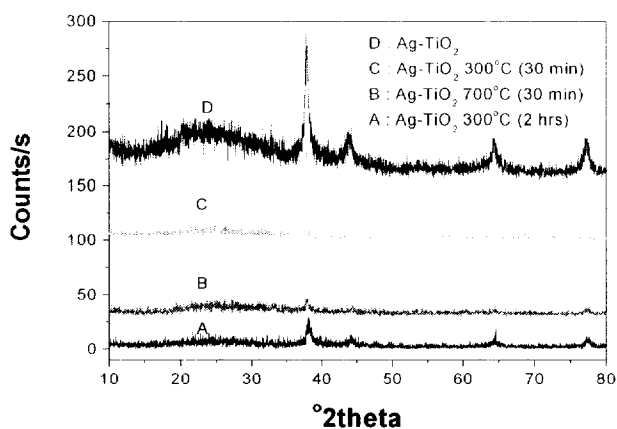


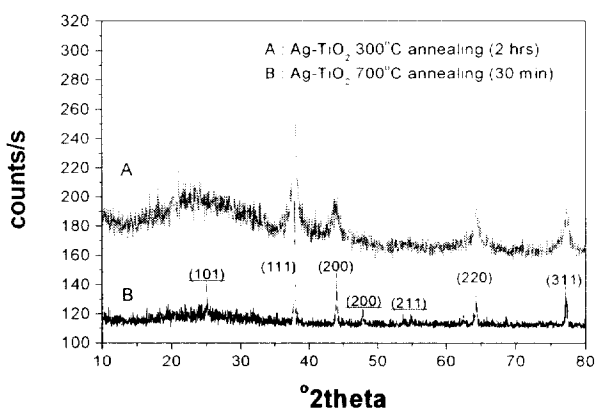
Figure 3. 19 UV-vis spectra of Ag nanoparticles ( $\lambda_{\text{max}} = 411$  nm, A) and Ag-  $\text{TiO}_2$  nanoparticles ( $\lambda_{\text{max}} = 486$  nm, B).

#### 3-2-2-4. XRD

As shown in Figure 3, 20, the shell of  $\text{TiO}_2$  is amorphous at room temperature. So there are no XRD peaks of  $\text{TiO}_2$  (A). Upon heating the nanoparticles to  $300^\circ\text{C}$  for 30 min and 2 hrs, the peaks of  $\text{TiO}_2$  are not shown (B and D) too. ; diffractions due to  $\text{TiO}_2$  are still not presented. However, upon heating the nanoparticles to  $700^\circ\text{C}$  for 30 min, a pattern of anatase titanium and silver appears (C).<sup>71</sup> Figure 3. 20 (b) shows this nanoparticles composed of two components ; silver and anatase titanium. Four peaks at  $2\theta$  values of  $38.2^\circ$ ,  $44.5^\circ$ ,  $64.5^\circ$  and  $77.7^\circ$  correspond to (111), (200), (220) and (311) planes of silver, respectively and three peaks at  $2\theta$  values of  $25.2^\circ$ ,  $47.8^\circ$  and  $54.8^\circ$  correspond to (101), (200) and (211) planes of anatase titanium oxide, respectively (JCPDS, silver file no. 01-1164 and anatase titanium oxide file no. 71-1169).



(a)



(b)

Figure 3. 20 X-ray diffraction pattern (Cu K $\alpha$ -radiation) of Ag-TiO<sub>2</sub> nanoparticles at annealing time and temperature (a) and confirmed with JCPDS cards (silver file no. 01-1164 and anatase titanium oxide file no 71-1169, underlined part) (b).

### 3-2-2-5. EDX

Two energy dispersive X-ray (EDX) data in Figure 3. 21 show that this nanoparticles consist of Ag and Ti components. Before oleic acid coating

and sonication treatment, the atomic ratio of Ag is 62.36 and Ti is 37.64, but after oleic acid coating and sonication treatment, the atomic ratio of Ag is 79.77 and Ti is 20.23 (Table 1).  $\text{TiO}_2$  nanoparticle layer on surface of Ag nanoparticles are partially eliminated by oleic acid coating and sonication treatment. So atomic ratio of Ag to Ti increased.

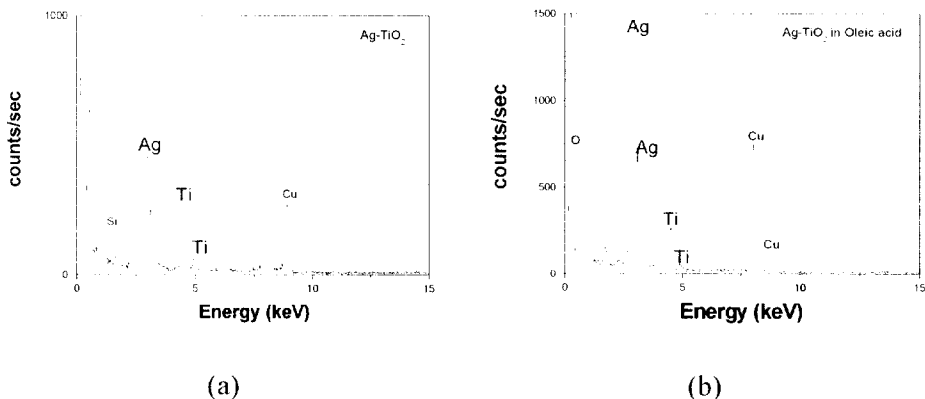


Figure 3. 21 Energy-dispersive X-ray spectra of Ag- $\text{TiO}_2$  before oleic acid coating and sonication (a) and after it (b).

**Table 3. 3 Element and atomic ratio of Ag- $\text{TiO}_2$  nanoparticles before oleic acid coating and sonication treatment.**

	Before oleic acid coating and sonication treatment		After oleic acid coating and sonication treatment	
	Element (%)	Atomic (%)	Element (%)	Atomic (%)
Ti	21.14	37.64	4.06	20.23
Ag	78.86	62.36	95.94	79.77
Total	100.00	100.00	100.00	100.00

### 3-3. Synthesized Ag- $\text{SiO}_2$ nanoparticles

#### 3-3-1. TEM

Figure 3. 22 showed TEM image of Ag- $\text{SiO}_2$  nanoparticles whose  $\text{SiO}_2$  nanoparticle size was about 200 nm and Ag nanoparticle size was below 10



nm. TEM image shows  $\text{SiO}_2$  nanoparticles were homogeneously impregnated with Ag nanoparticles. Fixing ratio of  $\text{SiO}_2$ , we controlled the ratio of  $\text{AgNO}_3$ . As the concentration of  $\text{AgNO}_3$  increased, the number of Ag nanoparticles which was deposited on the surface of  $\text{SiO}_2$  increased and the size of Ag nanoparticles increased.

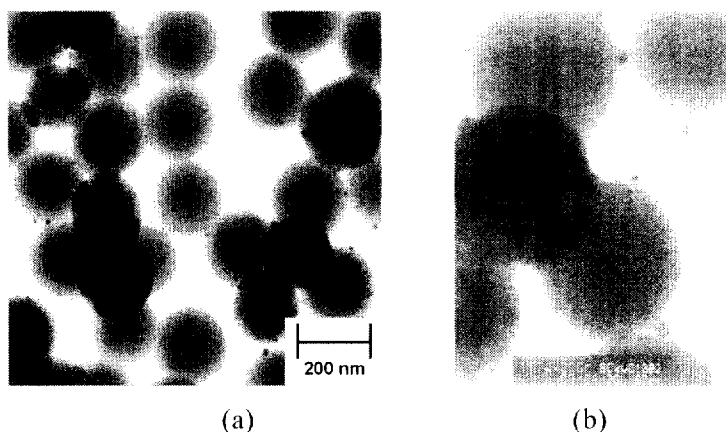


Figure 3. 22 TEM image of Ag- $\text{SiO}_2$  nanoparticle : (a)  $\text{SiO}_2$  nanoparticle size is determined as about 200 nm and (b) Ag nanoparticle size is below 10 nm.

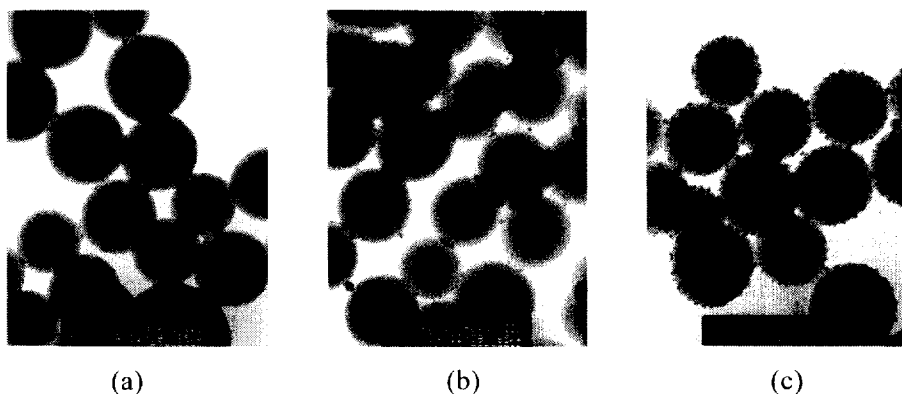


Figure 3. 23 Ag- $\text{SiO}_2$  nanoparticles prepared with different  $\text{AgNO}_3$ . (a) Ag :  $\text{SiO}_2$  = 1 : 1, (b) Ag :  $\text{SiO}_2$  = 2 : 1, and (c) Ag :  $\text{SiO}_2$  = 3 : 1.

### 3-3-2. High Resolution TEM images

We investigated the morphology with high resolution TEM. Very even

Ag nanoparticles deposited on the surface of  $\text{SiO}_2$  nanoparticles were prepared in water but not in ethanol.

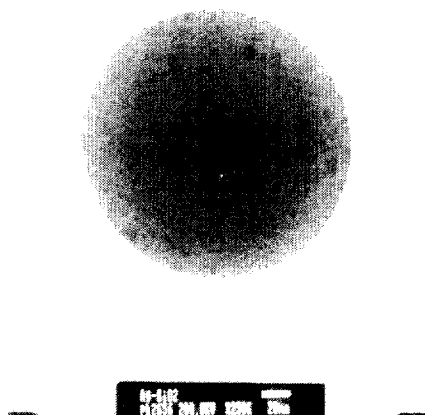


Figure 3. 24 M-TEM image of  $\text{SiO}_2$  nanoparticle deposited Ag nanoparticles.

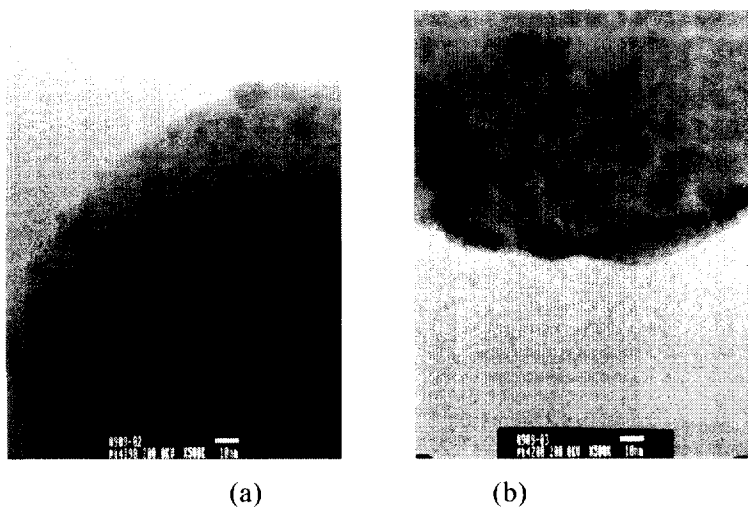


Figure 3. 25 Ag- $\text{SiO}_2$  nanoparticles prepared in water (a) and ethanol (b).

### 3-3-3. UV-vis

UV-vis spectrum of Ag- $\text{SiO}_2$  nanoparticle was also shown in Figure 3. 26. UV-vis spectrum of Ag- $\text{SiO}_2$  nanoparticle showed absorption band at 420

nm where as UV-vis spectrum of Ag nanoparticles prepared showed  $\lambda_{\max}$  at 410 nm. This absorption band was broad and red-shifted compared with the plasmon absorption band of Ag nanoparticle. As discussed earlier, the position and shape of the plasmon absorption of silver nanoparticles were strongly dependent on the particle size, dielectric medium, and surface-adsorbed species. This was concerned with red-shifted absorption band of Ag-SiO<sub>2</sub>.<sup>69-70</sup>

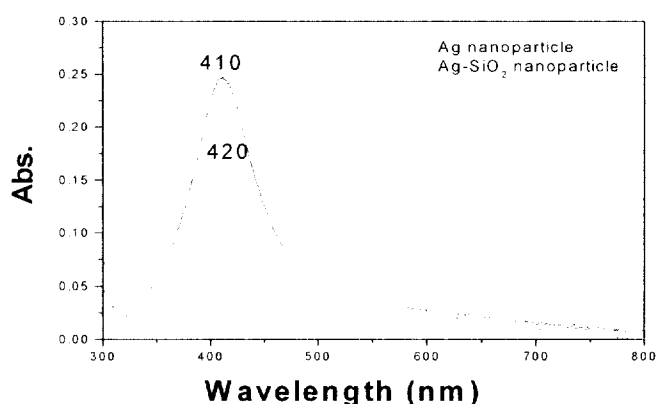


Figure 3. 26 UV-vis spectra of Ag nanoparticle ( $\lambda_{\max} = 410$  nm) and Ag-SiO<sub>2</sub> nanoparticle ( $\lambda_{\max} = 420$  nm).

### 3-2-4. EDS

#### 3-3-4-1. TEM-EDS

EDX spectrum of Figure 3. 27 showed that this product consisted of Ag and Si components. We investigated the atomic ratio of Ag to Si of Ag-SiO<sub>2</sub> nanoparticles with TEM-EDS. Since the area to be measured by TEM-EDS is very narrow, the ratio of Ag to Si not increased with increasing the mounts of AgNO<sub>3</sub>.

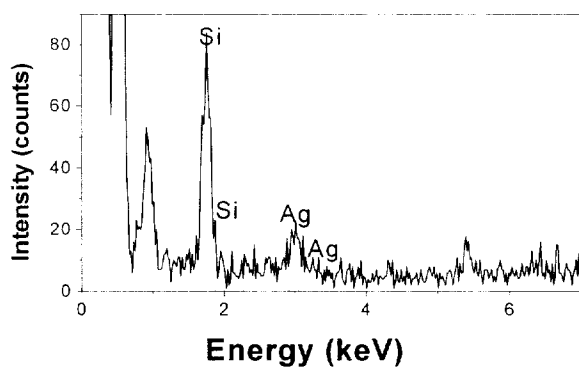


Figure 3. 27 Energy-dispersive X-ray spectrum of Ag-SiO<sub>2</sub> nanoparticles.

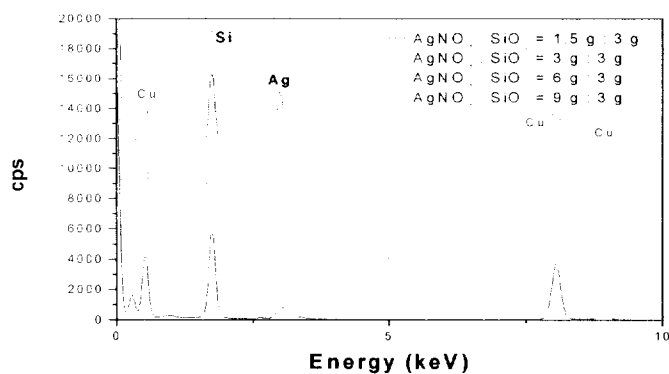


Figure 3. 28. TEM-EDS data of Ag-SiO<sub>2</sub> nanoparticles.

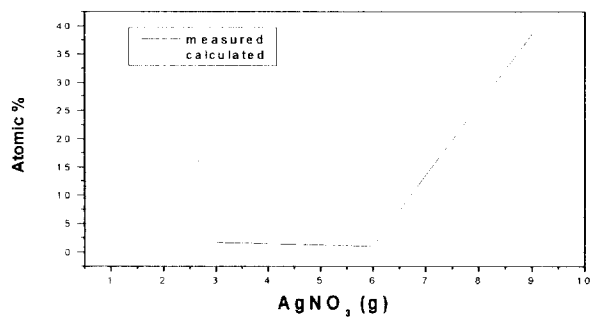


Figure 3. 29 Measured and calculated value of Ag-SiO<sub>2</sub>.

**Table 3. 4 Ag and Si atomic% of Ag-SiO<sub>2</sub> nanoparticles.**

	input (g)		EDS data (atomic %)	
	Ag	Si	Ag	Si
1	1.5	3	11.95	88.05
2	3	3	1.66	98.34
3	6	3	1.06	98.94
4	9	3	38.58	61.42

### 3-3-4-2. SEM-EDS

Although SEM-EDS was investigated on the larger area than TEM-EDS, the measured value of the ratio of Ag to Si was different from the calculated value of the ratio of Ag to Si.

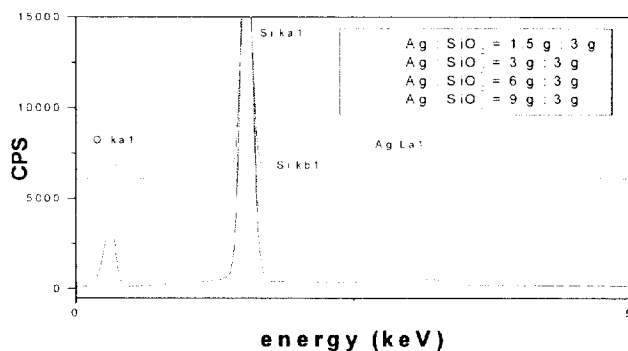


Figure 3. 30 SEM-EDS data of Ag-SiO<sub>2</sub> nanoparticles.

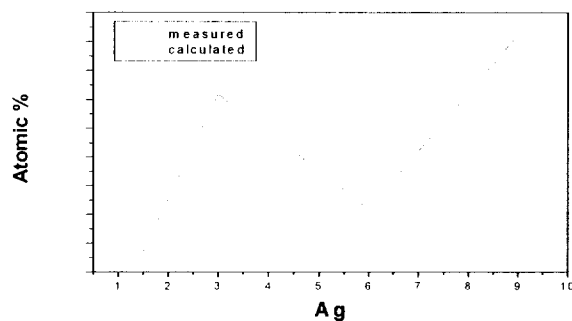


Figure 3. 31 Measured and calculated value of Ag-SiO<sub>2</sub> of SEM-EDS.

**Table 3. 5 Ag and Si atomic% of Ag-SiO<sub>2</sub> nanoparticles of SEM-EDS.**

	input (g)		EDS data (atomic %)	
	Ag	Si	Ag	Si
1	1.5	3	5.36	94.64
2	3	3	8.09	91.91
3	6	3	6.10	93.90
4	9	3	9.13	90.87

### 3-4. Synthesized Cu nanoparticles

#### 3-4-1. TGA

The decomposition path of the Cu-oleate complexes was studied by TGA analysis. Figure 3. 32 shows weight loss of Cu-oleate complexes during heat treatment under air flow. Very strong endothermic peaks were observed at about 290 °C and 480 °C in all different oleate concentrations. The peaks result from the decomposition of Cu-oleate. The first and second weight loss steps in the TGA curve might attribute to the releases of the outer and inner oleate layers, respectively.<sup>63</sup> Figure 3. 33 shows the formation of inner and outer layer of Cu-oleate complex. Similar suggestion also was proposed by Nikoobakht and El-sayed.<sup>72</sup> In this study, we used sodium oleate as capping agents to protect from oxidation of Cu nanoparticles because oleate has a C<sub>18</sub>(oleic) tail with a cis-double bond in the middle, forming a kink. Such kinks have been postulated as necessary for effective stabilization, but stearic acid (CH<sub>3</sub>(CH<sub>2</sub>)<sub>16</sub>COOH) without double-bond in its C<sub>18</sub> tail, cannot stabilize suspensions.<sup>73</sup>

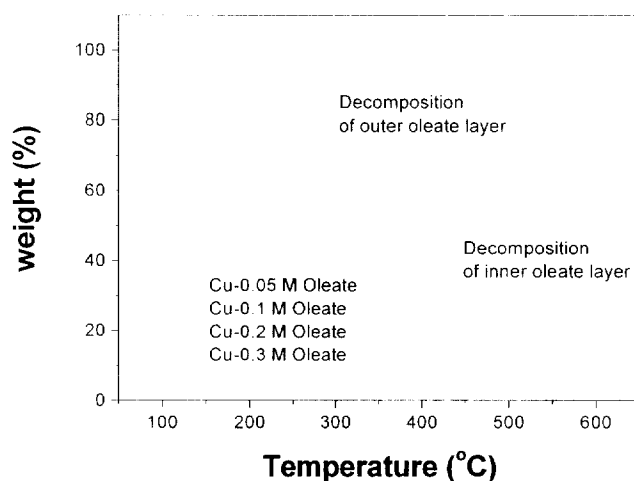


Figure 3. 32 TGA curves of different Cu-oleate complexes during heat treatment under air flow.

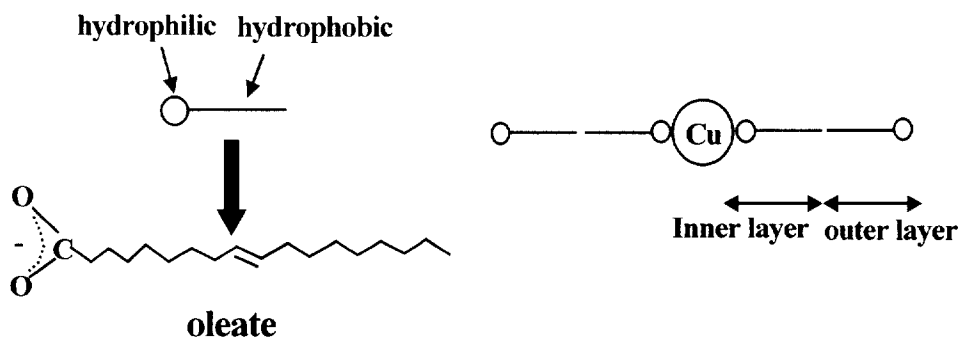


Figure 3. 33 The formation of inner and outer layers of Cu-oleate complex.

### 3-4-2. TEM

Figure 3. 34 shows TEM images of nanocrystallite of copper at different oleate concentrations. At the oleate of 0.05 M (a), the diameter is  $16.2 \pm 2.9$  nm and the particles are well dispersed and spherical. At the oleate of 0.1 M and 0.2 M, the diameters of Cu nanoparticles increase slightly with increasing oleate concentration. In these two oleate concentrations, Cu

nanoparticles are dispersed, although a few lumps present. These lumps of coalesced nanoparticles partly be formed on the grid. The diameters of Cu nanoparticle at 0.1 M (b) and 0.2 M (c) oleate concentration are  $21.4 \pm 2.3$  nm and  $24.3 \pm 1.9$  nm, respectively. At the 0.3 M (d) oleate concentration, the diameter of Cu nanoparticles is determined as 30.9 nm and a very broad distribution of size (6.4 nm) is observed. At high oleate concentration, large lumps are formed because of the coalescence of destabilized nanoparticles.<sup>74</sup>

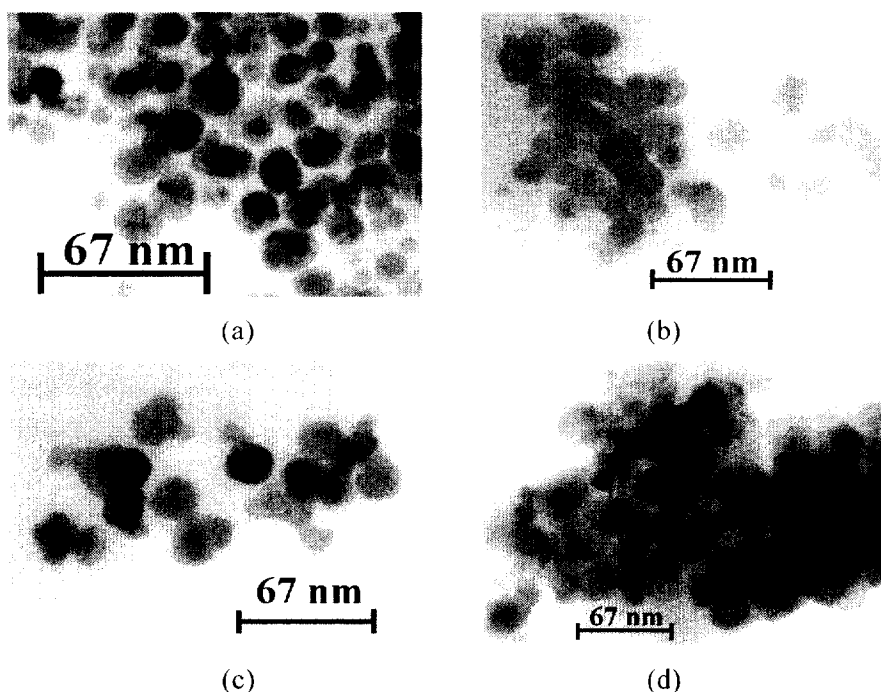


Figure 3. 34 Transmission electron micrographs of copper nanoparticles at different oleate concentrations. (a) at the oleate concentration of 0.05 M, (b) 0.1 M, (c) 0.2 M and (d) 0.3 M



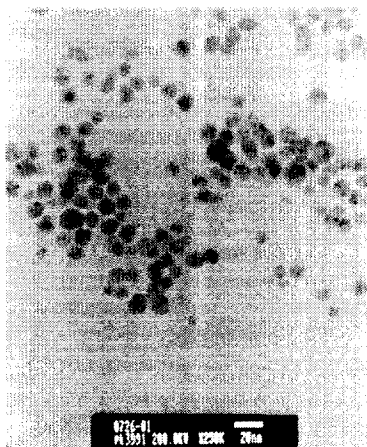


Figure 3. 35 Transmission electron micrographs of copper nanoparticles at the oleate concentraton of 0.05 M.

The particles size is determined as  $8.9 \pm 1.3$  nm

#### 3-4-3. XRD

The Figure 3. 36 illustrates the XRD pattern of aging of Cu-oleate (0.1 M) complex at 300 °C. The signature of copper is observed during the aging of Cu-oleate complex at 300 °C. Peaks are very sharp due to the high nanocrystalline nature of copper. Three peaks at  $2\theta$  values of 43.3 °, 50.4 ° and 74.1 ° correspond to (111), (200) and (220) planes of copper, respectively. (JCPDS, copper file no. 04-0836). No impurity peak is observed in the X-ray diffraction pattern.

#### 3-4-4. EDX

Figure 3. 37 shows the EDX spectra of copper nanoparticles excited by an electron beam (120 kV). Peaks for the elements of Cu and C were observed at 0.9297 ( $\text{Cu}_{\text{La}}$ ), 8.0477 ( $\text{Cu}_{\text{Ka}}$ ), 8.905 ( $\text{Cu}_{\text{Kb}}$ ), and 0.2774 ( $\text{C}_{\text{Ka}}$ ). There is no impurity atom in the nanoparticles except copper atom. Accordingly, from the EDX spectra we could confirm that the nanoparticles are pure copper.

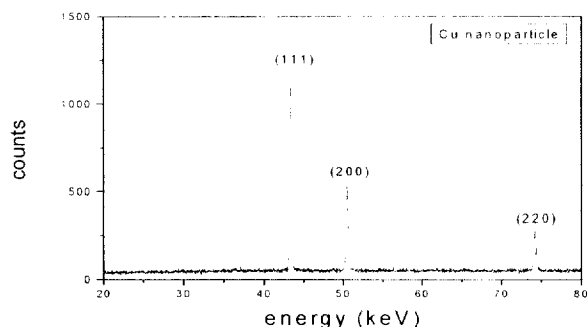


Figure 3. 36 X-ray diffraction pattern ( $\text{Cu}_{\text{K}\alpha}$ -radiation) of copper nanoparticles.

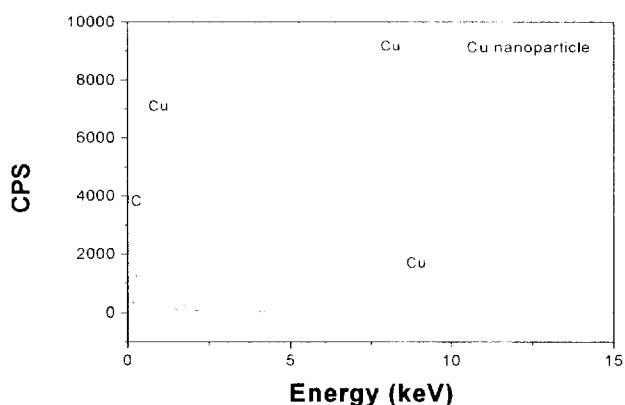


Figure 3. 37 Energy-dispersive X-ray spectra of copper nanocrystallites.

### 3-5. Antibiotic test

#### 3-5-1. Ag nanoparticles

Figure 3. 38 shows antibiotic property of Ag nanoparticles and there is no bacteria on the transparent circle. We put directly Ag nanoparticles instead of disk. As the antibiotic property increase, the transparent circles increase. The antibiotic properties of Ag nanoparticles with *Escherichia Coli* IOF 3972 and *Staphylococcus Aureus* IFO 12732 show good results because the

transparent circles is observed.

### 3-5-2. $\text{TiO}_2$ nanoparticles

As  $\text{TiO}_2$  nanoparticles is photocatalyst, so  $\text{TiO}_2$  is required light to display antibiotic properties, but usually antibiotic test is carried out in the case of excluding light. Figure shows that there is no antibiotic properties.

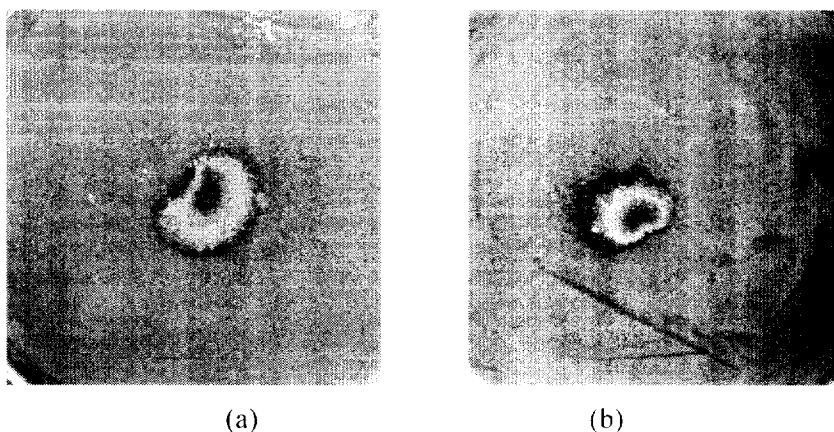


Figure 3. 38 Antibiotic test of Ag nanoparticles.

(a) Escherichia Coli IOF 3972 (b) Staphylococcus Aureus IFO 12732

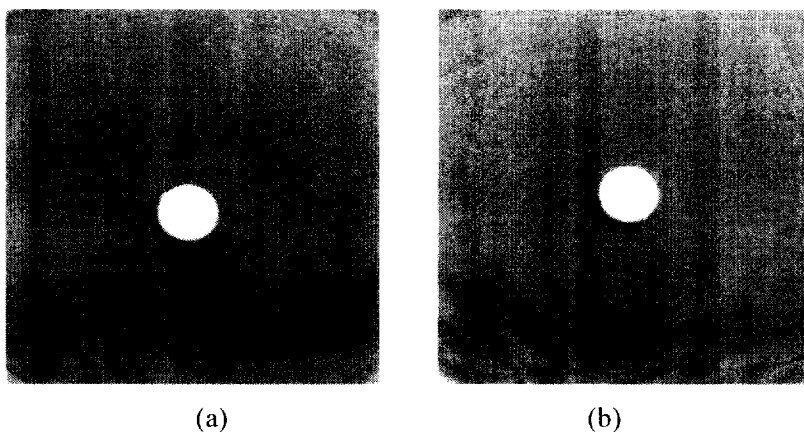


Figure 3. 39 Antibiotic test of  $\text{TiO}_2$  nanoparticle.

(a) Escherichia Coli (b) Staphylococcus Aureus

### 3-5-3. Ag- $\text{TiO}_2$

As Ag nanoparticles are coated with TiO<sub>2</sub> nanoparticles, there is no antibiotic properties because of the same reason of TiO<sub>2</sub>.

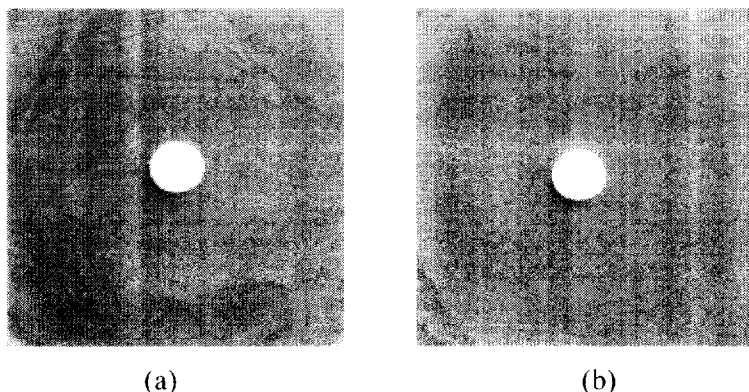


Figure 3. 40 Antibiotic test of Ag-TiO<sub>2</sub> nanoparticle.  
(a) Escherichia Coli and (b) Staphylococcus Aureus

#### 3-5-4. Ag-SiO<sub>2</sub>

The second antibiotic method is paper disk (8 mm) method (50 µl) and test bacteria are Pseudomonas Aeruginosa, Staphylococcus Aureus, Escherichia Coli, Enterobacter Cloacae, Candidaalbicans, Penicillium Citrinum and Aspergillus Niger. Antibiotic results of Ag-SiO<sub>2</sub> nanoparticles are shown in Table 3. 6 and Figure 3. 41. Numbers in parenthesis are the percent of Ag in Ag-SiO<sub>2</sub> nanoparticles.

**Table 3. 6 Clear Zone Value of Ag-SiO<sub>2</sub>.**

	1 (24.09%)	2 (38.83%)	3 (55.94%)	4 (65.58%)	note
S. Aureus	9.0	9.0	9.0	10.0	unit : mm
P. Aeruginosa	14.0	13.0	13.0	13.5	
E. Coli	-	-	-	-	
Ent. Cloacae	-	-	-	-	
C. Albicans	+	+	+	11.0	
P. Citrinum	-	+	+	11.5	
A. Niger	-	-	-	+	

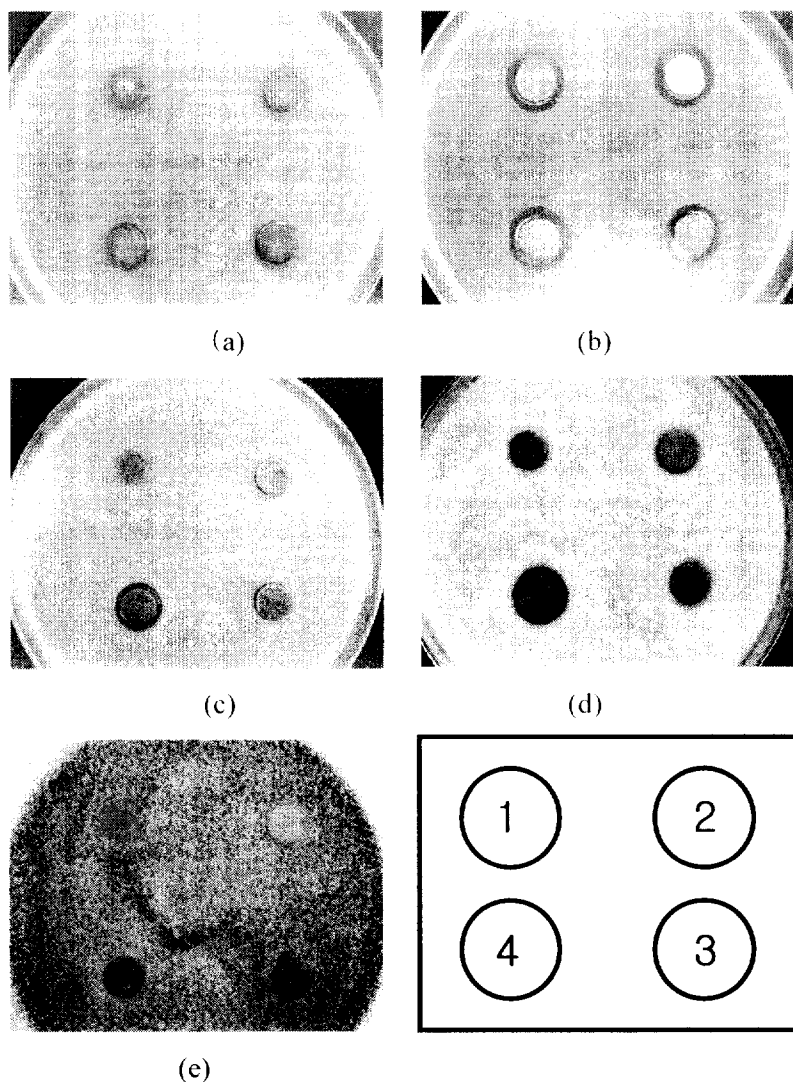


Figure 3. 4l Clear zone figure of Ag-SiO<sub>2</sub>.

(a) *S. aureus*, (b) *P. aeruginosa*, (c) *C. albicans*, (d) *P. citrinum* and  
(e) *A. niger*

Test samples are dissolved in ethanol and made 5% (W/V) and the Ag concentration of Ag-SiO<sub>2</sub> nanoparticles is shown in Table 3. 7. Number 4 has the most antibiotic properties in all samples except *E. coli*. and *Ent. cloacae*

**Table 3. 7 Ag concentration of Ag-SiO<sub>2</sub> nanoparticles.**

No.	1	2	3	4
Ag concentration (%)	24.09	38.83	55.94	65.58

**Table 3. 8 The results of antibiotic properties of Ag-SiO<sub>2</sub> concentration.**

	0	1	2	3	4	5	6	7	8
	0.0	0.01	0.02	0.03	0.05	0.1	0.2	0.3	0.5
Escherichia coli	+	+	+	-	-	-	-	-	-
Pseudomonas aeruginosa	+	+	+	-	-	-	-	-	-
Staphylococcus aureus	+	+	+	+	+	-	-	-	-
Enterobacter cloacae	+	+	+	+	+	+	+	+	-
Candida albicans	+	+	+	+	+	+	-	-	-
Penicillium citrinum	+	+	+	+	+	-	-	-	-
Aspergillus niger	-	+	+	+	+	-	-	-	-

Antibiotic test method (MIC, minimum inhibition concentration) of Ag-SiO<sub>2</sub> Nanoparticle is plate dilution method and test bacteria are Pseudomonas aeruginosa, Staphylococcus aureus, Escherichia coli, Enterobacter cloacae, Candida albicans, Penicillium citrinum and Aspergillus niger. The MIC range of AgSiO<sub>2</sub> nanoparticle is from 0.03 to 0.5%.

**Table 3. 9 MIC (%) of Ag-SiO<sub>2</sub> nanoparticles in various bacteria.**

bacteria	MIC (%)
Escherichia coli	0.05 - 0.10
Pseudomonas aeruginosa	0.02 - 0.03
Staphylococcus aureus	0.05 - 0.10
Enterobacter cloacae	0.3 - 0.5
Candida albicans	0.1 - 0.2
Penicillium citrinum	0.1 - 0.2
Aspergillus niger	0.1 - 0.2

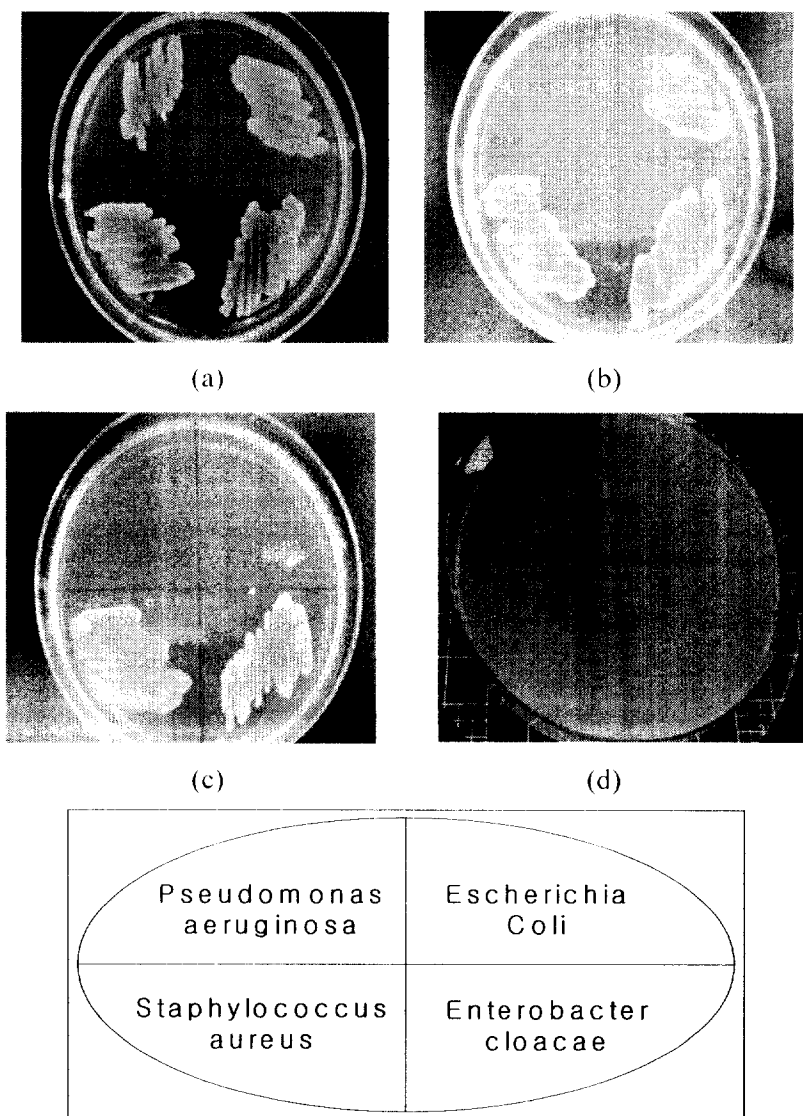


Figure 3. 42 The result of antibiotic properties of Ag-SiO<sub>2</sub> nanoparticles  
the concentration of Ag-SiO<sub>2</sub> nanoparticles : (a) : 0.02%; (b) : 0.03%;  
(c) : 0.05% and (d) : 0.5%

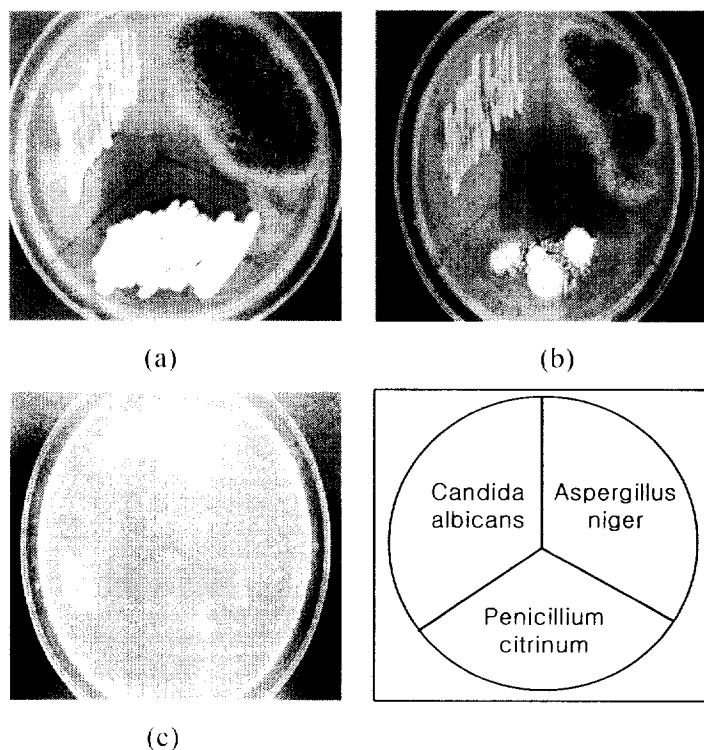


Figure 3. 43 The result of antibiotic properties of Ag-SiO<sub>2</sub> nanoparticles. the concentration of Ag-SiO<sub>2</sub> nanoparticles ; (a): 0.05%; (b): 0.1%; and (c):0.2%

### 3-5-5. Antibiotic property using UV-vis spectroscopy

The behavior of bacteria using absorption of UV-vis at 640 nm was investigated. If there is antibiotic materials, the absorption spectrum is low. Figure 3. 44 shows that Ag nanoparticle is the highest antibiotic materials but there is no antibiotic property at low concentration (0.2 g/200 ml) In case of TiO<sub>2</sub> nanoparticles, there is antibiotic property in case of G but there is no antibiotic property in case of F. In case of antibiotic test of TiO<sub>2</sub> nanoparticles using disk, there is no antibiotic property, but in case of antibiotic test of TiO<sub>2</sub> nanoparticles using UV-vis, there is antibiotic property because of light. As light is forbidden in case of antibiotic test of TiO<sub>2</sub> nanoparticles using disk, so antibiotic property is not detected because TiO<sub>2</sub>



is a photocatalyst. Since light is allowed in case of antibiotic test of  $\text{TiO}_2$  nanoparticles using UV-vis spectroscopy, antibiotic property is detected. In case of  $\text{Ag-TiO}_2$  nanoparticles, there is no antibiotic property.

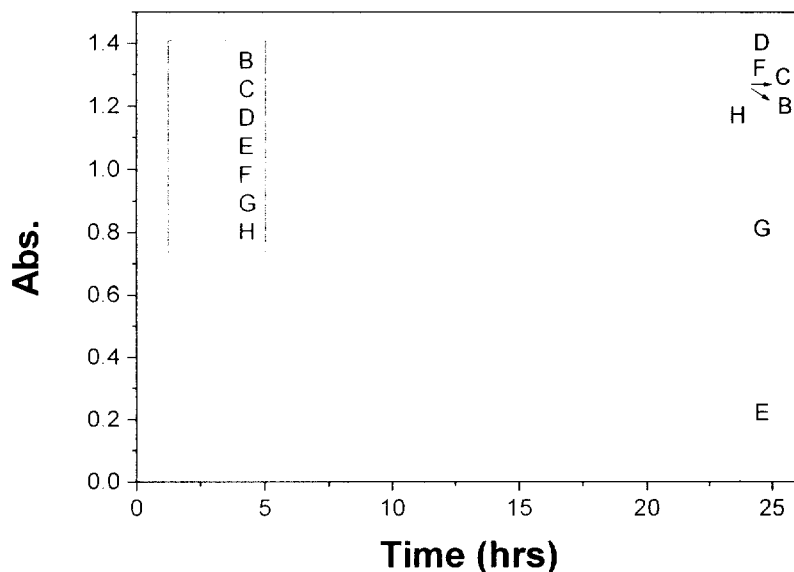


Figure 3. 44 Antibiotic test using UV-vis.

B : bacterium, C : bacterium, D : Ag nanoparticle (0.2 g/200 ml) + bacterium, E : Ag nanoparticle (2 g/200 ml) + bacterium, F :  $\text{TiO}_2$  nanoparticle (0.02 g/200 ml) + bacterium, G :  $\text{TiO}_2$  nanoparticle (0.2 g/200 ml) + bacterium and H :  $\text{Ag-TiO}_2$  nanoparticle (0.2 g/200 ml) + bacterium.

### 3-6. Deodorant test

#### 3-6-1. Valeric acid

We investigated deodorant test with the peak of GC using valeric acid known as the main factor of the stink of the feet. The retention time of valeric acid is about 1.8 min (1 min 50 second). The value from the area of peak is calculated and spontaneous decrease percent is shown in the

table. After 24 hrs, the decrease in value is 16.8% compared to that of 0 hrs.

**Table 3. 10 Value of area and percent of decrease of valeric acid in the passage of time.**

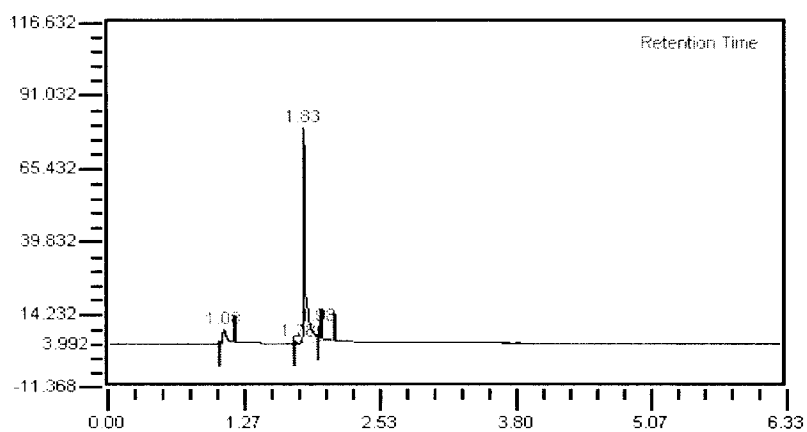
Time	0	8	16	24
Area	2325064	2340511	2317097	1934930
percent of decrease		0.01%	0.3%	16.8%

### 3-6-2. $\text{TiO}_2$

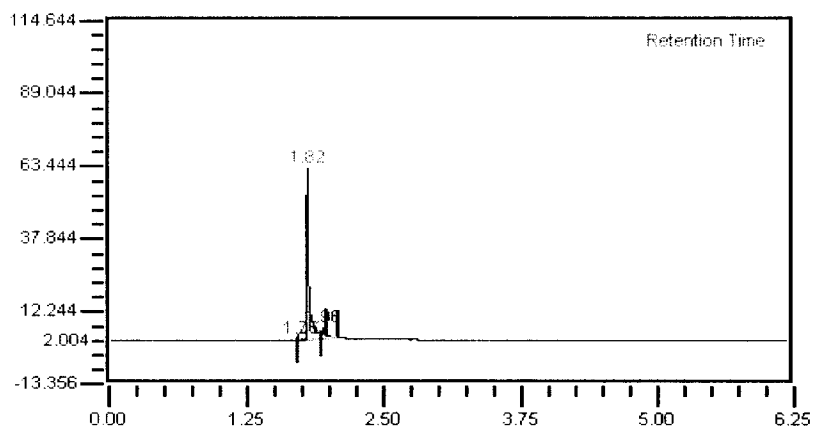
$\text{TiO}_2$  is a good deodorant materials in early state because the percent of decrease is 77.8% after 8 hrs. The percent of decrease is 83.9% after 16 hrs and 88.1% after 24 hrs.

**Table 3. 11 Value of area and percent of decrease of valeric acid contained  $\text{TiO}_2$  nanoparticles in the passage of time.**

Time	00	08	18	24
Area	9887891	2225001	1592913	1174755
percent of decrease		77.5%	83.9%	88.1%



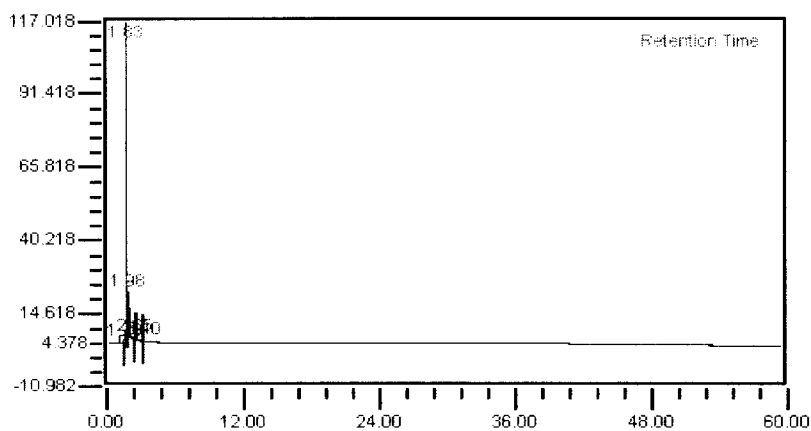
(a)



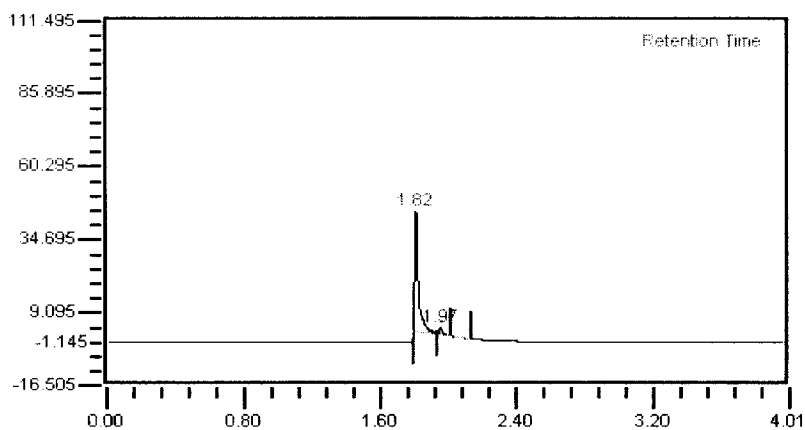
(b)

Figure 3. 45 Decrease of peak of valeric acid in the passage of time.

(a) : 0 hrs and (b) : 24 hrs



(a)



(b)

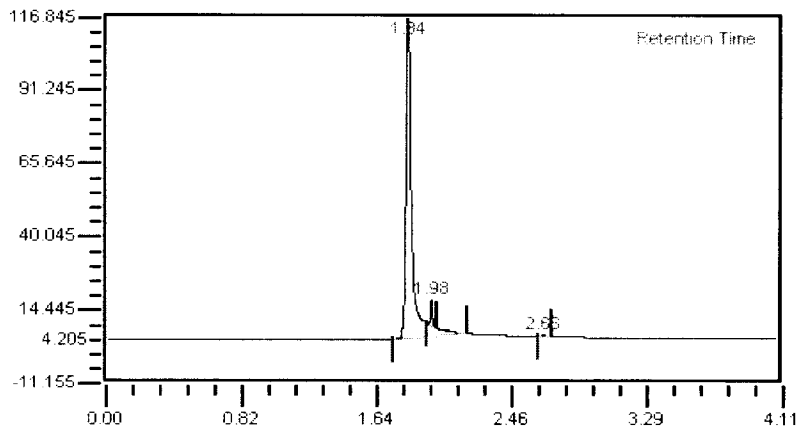
Figure 3. 46 Decrease of peak of valeric acid contained  $\text{TiO}_2$  nanoparticles in the passage of time.

(a) : 0 hrs and (b) : 24 hrs

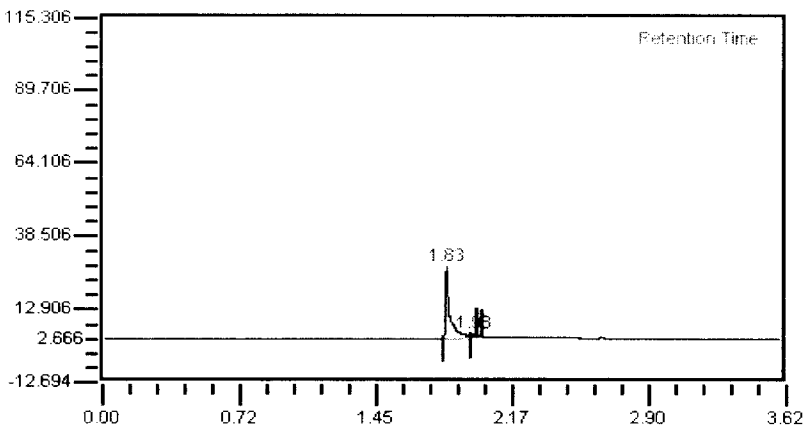
### 3-6-3. Ag- $\text{TiO}_2$

Although the deodorant property of Ag- $\text{TiO}_2$  nanoparticles is weaker than that of  $\text{TiO}_2$  in early state, the percent of decrease of Ag- $\text{TiO}_2$  nanoparticles

after 24 hrs is same as that of TiO<sub>2</sub> nanoparticles.



(a)



(b)

Figure 3. 47 Decrease of peak of valeric acid contained Ag-TiO<sub>2</sub> nanoparticles in the passage of time.  
(a) : 0 hrs and (b) : 24 hrs

**Table 3. 12 Value of area and percent of decrease of valeric acid contained Ag-TiO<sub>2</sub> nanoparticles in the passage of time.**

Time	00	08	16	24
Area	8005135	3426927	2755300	1046972
percent of decrease		57.2%	65.6%	86.9%

## 4. Conclusion

A new synthetic methods of Ag and Cu nanoparticles have been discovered to produce spherical and monodispersed silver and copper nanoparticles using thermal decomposition of Ag-oleate complex and Cu-oleate complex, and have core (metal) and shell (organic) shape. No extra inert gases protecting from the oxidation of Ag and Cu nanoparticles were necessary. By TGA measurement, thermal decompositions of Ag-oleate and Cu-oleate complexes were observed at about 295 and 290 °C, respectively. TEM images show that monodispersed silver nanoparticles are very regularly packed and are about 10 nm diameter. At 0.05 M oleate concentration, spherical copper nanoparticles ( $16.2 \pm 2.9$  nm) are prepared, but at high concentration (0.3 M), large lumps are formed. This method could be easily scaled up for industrial purpose. These nanoparticles are very pure silver and copper. Ag-TiO<sub>2</sub> nanoparticles are synthesized by sol-gel process using Ag nanoparticles as core seed. TEM images shows core (Ag)-shell (TiO<sub>2</sub>) structure and diameter of Ag core is about 13 nm and thickness of TiO<sub>2</sub> layer is less than 3 nm. UV-vis spectroscopy of core-shell type Ag-TiO<sub>2</sub> nanoparticles shows a large red-shift of the silver plasmon band from 411 nm, which is typical for uncoated silver nanoparticles, to 486 nm. In XRD peaks of Ag-TiO<sub>2</sub> nanoparticles, the crystalline structure of TiO<sub>2</sub> layer increased with increasing annealing temperature and time. This is obviously shown by XRD peaks of TiO<sub>2</sub> in Ag-TiO<sub>2</sub> nanoparticles. EDX also shows that the nanoparticles comprises two components ; Ag and Ti. After and before oleic acid coating and sonication, there are different results of TEM, ED and EDS because of partial TiO<sub>2</sub> layer desorption. Ag-SiO<sub>2</sub> nanoparticle prepared by using well-known Stöber method is carried out at room temperature. This method is well suited for preparing metal nanoparticle coatings on monodisperse silica nanoparticle without the chemical aids usually applied to achieve particulate coatings. In

antibiotic and deodorant test of these synthesized nanoparticles. Ag and Ag-SiO<sub>2</sub> have good antibiotic property and Ag-TiO<sub>2</sub> has good deodorant property.



## 5. References

1. Drexler, K. E. *Sci. Am.* **2001**, 74, 285.
2. Spurgeon, D. *Nature* **2001**, 412, 846.
3. Forrest, D. R. *IEEE Instrum. Meas. Mag.* **2001**, 4, 11.
4. Forster, S.; Antonietti, M. *Adv. Mater.* **1998**, 10, 195.
5. Moffit, M.; Eisenberg, A. *Chem. Mater.* **1995**, 7, 1178.
6. Ghosh, K.; Maiti, S. N. *J. Appl. Polym. Sci.* **1996**, 60, 323.
7. Andres, R. P.; Bielfeld, J. D.; Henderson, J. I. *Science* **1996**, 273, 1960.
8. Toshima, N.; Wang, Y. *Langmuir* **1994**, 10, 4574.
9. Henglein, A. *J. Phys. Chem.* **1993**, 97, 5457.
10. Hirai, H. *J. Macro. Sci. Chem.* **1979**, 633, 727.
11. Huang, H. H.; Ni, X. P.; Loy, G. H.; Chew, C. H.; Tan, K. L.; Loh, F. C.; Deng, J. F.; Xu, G. Q. *Langmuir* **1996**, 12, 909.
12. Okitsu, K.; Bandow, H.; Maeda, Y.; Nagata, Y. *Chem. Mater.* **1996**, 8, 315.
13. Janata, E. *Radiation Chemistry* **1996**, 47, 29.
14. Joshi, S. S.; Patil, S. F.; Lyer, V.; Mahumuni, S. *Nanostruct. Mater.* **1998**, 10, 1135.
15. Lisiecki, I.; Pileni, M. P. *J. Am. Chem. Soc.* **1993**, 115, 3887.
16. Ohde, H.; Hunt, F.; Wai, C. M. *Chem. Mater.* **2001**, 13, 4130.
17. Dhas, N. A.; Raj, C. P.; Gedanken, A. *Chem. Mater.* **1998**, 10, 1446.
18. Yeh, M. S.; Yang, Y. S.; Lee, Y. P.; Lee, H. F.; Yeh, Y. H.; Yeh, C. S. *J. Phys. Chem.* **1999**, 103, 6851.
19. Vitulli, G.; Bernini, M.; Bertozzi, S.; Pitzalis, E.; Salvadori, P.; Coluccia, S.; Martra, G. *Chem. Mater.* **2002**, 14, 1183.
20. Lisiecki, I.; Billoudet, F.; Pileni, M. P. *J. Phys. Chem.* **1996**, 100, 4160.
21. Li, Q. X.; Tang, H. A.; Li, Y. Z.; Wang, M.; Wang, L. F.; Xia, C. G. *J. Inorg. Biochem.* **2000**, 78, 167.
22. Haus, J. W.; Zhou, H. S.; Takami, S.; Hirasawa, M.; Honma, I.;

- Komiyama, H. *J. Appl. Phys.* **1993**, 73, 1043.
23. Giersig, M.; Liz-Marzan, L. M.; Ung, T.; Su, D.; Mulvaney, P. Ber. Bunsenges. *Phys. Chem.* **1997**, 101, 1617.
  24. Westcott, S.; Oldenburg, S.; Lee, T. R.; Halas, N. J. *Langmuir* **1998**, 14, 5396.
  25. Averitt, R. D.; Sarkar, D.; Halas, N. J. *Phys. Rev. Lett.* **1997**, 78, 4217.
  26. Oldenburg, S.; Averitt, R. D.; Westcott, S.; Halas, N. J. *Chem. Phys. Lett.* **1998**, 288, 243.
  27. Westcott, S.; Oldenburg, S.; Lee, T. R.; Halas, N. J. *Chem. Phys. Lett.* **1999**, 300, 651.
  28. Averitt, R. D.; Westcott, S.; Halas, N. J. *J. Opt. Soc. Am.* **1999**, 16, 1824.
  29. Serksen, S. R.; Westcott, S. L.; Halas, N. J.; West, J. L. *J. Biomed. Mater. Res.* **2000**, 51, 293.
  30. Jackson, J. B.; Halas, N. J. *Silver nanoshells: J. Phys. Chem B* **2000**, 105, 2743.
  31. Mayoral, R.; Requena, J.; Moya, J. S.; Lopez, C.; Ciontas, A.; Miguez, H.; Meseguer, F.; Vazquez, L.; Holgado, M.; Blanco, A. *Adv. Mater.* **1997**, 9, 257.
  32. Rogach, O. E.; Kornowski, A.; Kapitonov, A. M.; Gaponenko, N. V.; Gaponenko, S. V.; Eychmüller, A.; Rogach, A. L. *Mater. Sci. Eng. B* **1999**, 64, 64.
  33. Romanov, S. G.; Sotomayor-Torres, C. M. *Three-dimensional Lattices of Nanostructures: The Template Approach*. in H. S. Nalwa (ed.): *Handbook of Nanostructured Materials*. Academic Press, New York **2000**, 4, 232.
  34. Ogihara, T. *Hydrolysis of Metal Alkoxides in Homogeneous Solution*. in T. Sugimoto (ed.): *Fine Particles Synthesis, Characterization and Mechanisms of Growth*. Marcel Dekker, New York **2000**, 35.
  35. Yonezawa, Y.; Sato, T.; Kuroda, S.; Kuge, K. *J. Chem. Soc. Faraday Trans.* **1991**, 87, 1905.

36. Koudelka, M.; Sanchez, J.; Augustynski, J. *J. Phys. Chem.* **1982**, 86, 4277.
37. Okitsu, K.; Mizukoshi, Y.; Bandow, H.; Maeda, Y.; Yamamoto, T.; Nagata, Y. *Ultrasonics Sonochem.* **1996**, 3, S249.
38. Morke, W.; Lamber, R.; Schubert, U.; Breitscheidel, B. *Chem. Mater.* **1994**, 6, 1659.
39. Dreys, H.; Morke, W.; Jarsetz, J.; Bieruta, T.; Hofmeister, H. *Appl. Organomet. Chem.* **1998**, 12, 321.
40. Dokoutchaev, A.; James, J. T.; Koene, S. C.; Pathak, S.; Prakash, G. K. S.; Thompson, M. E. *Chem. Mater.* **1999**, 11, 2389.
41. Gomez, S.; Phillippo, K.; Colliere, V.; Chandret, B.; Senocq, F.; Lecante, P. *Chem. Commun.* **2000**, 19, 1945.
42. Templeton, A. C.; Pietron, J. J.; Murray, R. W.; Mulvaney, P. *J. Phys. Chem. B* **2000**, 104, 564.
43. Hodak, J.; Henglein, A.; Hartland, G. V. *J. Phys. Chem. B* **2000**, 104, 9954.
44. Miclea, P. T.; Morke, W.; Dreys, H.; Lehrack, K.; Hofmeister, H. *Metal Nanoparticles by Direct Reduction on Non-Planar Silica Substrates*, in D. S. Su, S. Wrabetz (eds.): *Proc. Autumn School Berlin 2000 Mat. Science & Electr. Microsc., Fritz Haber Institute, Berlin* **2000**, 63.
45. Mayer, A. B. R.; Grebner, W.; Wannemacher, R. *J. Phys. Chem. B* **2000**, 104, 7278.
46. Tobin, E. J.; Bambauer, R. *Therapeutic Apheresis and Dialysis*. **2003**, 7(6), 504.
47. Balogh, L.; Swanson, D. R.; Tomalia, D. A.; Hagnauer, G. L.; Mcmanus, A. T. *Nano Lett (Communication)* **2001**, 1(1), 18.
48. Hoffmann, M. R.; Martin, S. T.; Choi, W.; Behnemann, D. W. *Chem. Rev.* **1995**, 95, 69.
49. Richardson, S. D. *Environmental Sci. & Tech.* **1996**, 30(11), 3327.
50. Yu, J. C.; Ho, W.; Lin, J.; Yip, H.; Wong, P. K. *Environmental Sci & Tech.* **2003**, 37(10), 2296.

51. Yu, J. C.; Yu, J.; Ho, W. *Chemical Communications* **2001**, 19, 1942.
52. Hong, S. S.; Lee, M. S.; Kim, J. H.; Ahn, B. H.; Lim, K. T.; Lee, G. D. *J. Ind. Eng. Chem.* **2002**, 8(2), 150.
53. Stöber, W.; Fink, A.; Bohn, E. *J. Colloid Interf. Sci.* **1968**, 26, 62.
54. Bergsson, G.; Steingrímsson, O.; Thormar, H. *Antimicrob. Agents Chemother.* **1999**, 43, 2790.
55. Bergsson, G.; Arnfinnsson, S. M.; Steinfrimsson, O.; Thormar, H. *Antimicrob. Agents Chemother.* **1998**, 42, 2290.
56. Livage, M.; Henry, M.; Sanchez, C. *Sol-Gel Chemistry of Transition Metal Oxides in Progress in Solid State Chemistry* **1988**, 18, 259.
57. Hubert-Pfalzgraf, L. C. *New J. of Chem.* **1987**, 11, 663
58. Hartel, R. W.; Berglund, K. A. in *Better Ceramics Through Chemistry II, Mater. Res. Soc. Symp. Proc.* **1986**, 73, 633
59. Budd, K. D.; Dey, S. K.; Payne, D. A. *Brit. Ceram. Soc. Proc.* **1985**, 36, 107.
60. Livage, J.; Henry, M. in *Ultrastructure Processing of Advanced Ceramics* **1998**, 183
61. Sanchez, C.; Livage, J.; Henry, M.; Babonneau, F. *J. Non-Cryst. Solids* **1988**, 100, 65
62. Adams, R. W.; Bishop, E.; Martin, R. L.; Winter, G. *Aust. J. Chem.* **1966**, 19, 207
63. Wu, S. H.; Chen, D. H. *J. Colloid Interface Sci.* **2004**, 273, 165.
64. Magudapathy, P.; Gangopadhyay, B. K. *Physical B* **2001**, 299, 142.
65. George, C.; Konstantin, S.; Therese, M. C. *J. Phys. Chem.* **1996**, 100, 5166.
66. Rivas, L.; Sanchez-Cortes, S.; Garcia-Ramos, J. V.; Morcillo, G. *Langmuir* **2001**, 17, 574.
67. Huang, J. B.; Yang, R.; Zhu, B. Y.; He, X.; Fu, H. L. *Colloids and Surfaces.* **2000**, 174, 403.
68. Rafael, T.; Ronald, E. R.; Joseph, F.; Jacob, K. *Langmuir* **2000**, 16, 9117.

- 69. Mulvaney, P. *Langmuir* **1996**, 12, 788.
- 70. Kreibig, U.; Vollmer, M. *Optical Properties of Metal Clusters* **1995**
- 71. Renjis, T. T.; Nair, A. S.; Singh, N.; Aslam, M.; Nagendra, C. L.; Philip, R.; Vijayamohanan, K.; Pradeep, T. *Langmuir* **2003**, 19, 3439.
- 72. Nikoobakht, B.; El-Sayed, M. A. *Langmuir* **2001**, 17, 6368.
- 73. Tadmor, R.; Rosensweig, R. E.; Frey, J.; Klein, J. *Langmuir*, **2000**, 16, 9117.
- 74. Henglein, A.; Giersig, M. *J. Phys. Chem. B* **1999**, 103, 9533.

## 6. Korean abstract

핵(무기물)-껍질(유기물)형태의 Ag와 Cu 나노입자를 전기로(autoclave)를 이용하여 Ag-oleate와 Cu-oleate를 열분해하여 합성하였다. 합성된 Ag 나노입자는 핵(무기물)-껍질(무기물)의 구조를 가진 Ag-TiO<sub>2</sub> 나노입자의 핵으로 사용된다. TEM이미지에서 titanium oxide로 코팅된 Ag 나노입자의 형상을 볼 수 있다. 또한 UV-vis를 이용하여 분광학적 특성과 항균적 특성 등을 분석하였다. 실온에서 Hybrid형의 구조를 얻기위해 Ag 나노입자가 Si표면에 결합되는 방법을 소개한다. Silica 나노입자는 촉매로 암모니아를 사용하여 물과 에탄올의 혼합물에서 TEOS의 가수분해와 축합반응에 의한 Stöber 방법에 의하여 합성되고 AgNO<sub>3</sub>와 합성된 SiO<sub>2</sub> 나노입자의 반응에 의하여 Ag-SiO<sub>2</sub>가 합성된다. XRD로 반폭치와 결정면을, TEM으로 입자크기와 형태를 분석하였고 항균적 특성 등을 또한 분석하였다.